# Development of Drug Delivery System for Apigenin against Inflammatory Disease - Approach for Clinical Application of Natural Products -

July 2019

Midori YAMASAKI

# Development of Drug Delivery System for Apigenin against Inflammatory Disease - Approach for Clinical Application of Natural Products -

A Dissertation Submitted to
the Graduate school of Life and Environmental Sciences
the University of Tsukuba,
in Partial Fulfillment of the Requirements
for the Degree of Doctor of Philosophy in Environmental Studies
(Doctoral Program in Sustainable Environmental Studies)

Midori YAMASAKI

**Abstract**

The pathogenesis of inflammatory diseases is deeply influenced by environmental factors. Inflammatory bowel disease (IBD) is one of the examples of chronic refractory digestive disorder which is influenced by environmental factor. The major types of IBD are Crohn's disease (CD) and ulcerative colitis (UC). These disorders are categorized based on the site of inflammation, histological findings, and clinical symptoms. The most common symptoms are diarrhea, fever, and abdominal pain. The pathogenesis of IBD remains unknown. However, a possible cause is dysfunction of the immune system. Numerous studies suggested that several factors such as food, smoking, and gut microbiota, are involved in the progression of the disease. Although various therapeutic approaches are available, most clinical drugs are associated with the occurrence of adverse effects. Therefore, the development of a more specific and safe treatment options is urgently warranted.

Here, the author proposed formulation strategy is one of the important factors that maximize the therapeutic effects of natural products. Drug delivery systems (DDS) could maximize the value of drug seeds by improving their pharmacokinetic profiles and/or pharmacodynamic effects and reducing the incidence of adverse effects. In this study, the author demonstrated that liposome, one of the major formulations of DDS, could accumulate target inflamed tissue in the lungs and colon through an enhanced permeability and retention (EPR) effect. Nanosized particle modification and targetability of nanoparticles were focused on both lung and colon injury sites. Previous studies have indicated that extracts of natural products have a potential to improve refractory diseases, such as neurological diseases, cancer, and inflammatory diseases. Thus, the author wished to investigate the usefulness of natural product encapsulation in nanoparticles. Especially, several plants derived from North Africa and the Mediterranean have beneficial health

effects compared with plants derived from other regions of the world. It has been demonstrated that several components of natural products (e.g., polyphenols and flavonoids) prevent functional impairment of intestinal epithelial cells and inflammation of the lamina propria in experimental IBD model. This is achieved through direct anti-inflammatory effects and indirectly therapeutic effects, including improvement of the gut microbiome environment. Finally, Apigenin nanoparticle could be manufactured successfully, Apigenin and Apigenin nanoparticles showed strong anti- inflammatory effects in several genetic markers in LPS-stimulated RAW264.7 cell line model. In summary, DDS maximizes the value of drug seeds, the formulation approach of natural products for inflammatory disease is attractive strategy. Apigenin nanoparticle is promising therapeutic option for these refractory diseases.

**Table of Contents**

**List of Figures**

**List of Tables**

**Abbreviations and Acronyms**

IBD: inflammatory bowel disease

CD: Crohn's disease

UC: ulcerative colitis

DDS: drug delivery systems

EPR: enhanced permeability and retention

PUFA: polyunsaturated fatty acid

AhR: aryl hydrocarbon receptor

API: active pharmaceutical ingredients

MCT: monocrotaline

PH: pulmonary hypertension

PEG: polyethylene glycol

RES: reticuloendothelial system

FL: fluorescent

DSPC: 1,2-distearoyl-sn-glycero-3-phosphocholine

Chol: cholesterol

DSPE-PEG: N-(carbonyl-methoxypolyethyleneglycol 5000)-1,2-distearoyl-sn-glycero-3-phosphoethanolamine

DiR: 1,1′-dioctadecyl-3,3,3′,3′-tetramethylindotricarbocyanine iodide

POPC:1-palmitoyl-2-oleoyl-sn-glycero-3-phosphocholine

IVIS: *in vivo* imaging system

FITC: fluorescein isothiocyanate

ROS: reactive oxygen species

L-012: 8-amino-5-chloro-7-phenylpyrido[3,4-d]pyridazine-1,4-(2H,3H) dione

ROI: region of interest

Nlrp: NOD-like receptor family pyrin containing

ConA: concanavalin A

HPRT: hypoxanthine-guanine phosphoribosyltransferase

MPO: myeloperoxidase

PLGA: poly lactic-co-Glycolic Acid

DOTAP: 1,2-dioleoyloxy-3-trimethylammonium propane

EtOH: ethanol

PKC: protein kinase C

**List of Publications**

1. Yamasaki M, Muraki Y, Nishimoto Y, Murakawa Y, Matsuo T.
Fluorescence-labeled liposome accumulation in injured colon of a mouse model of T-cell transfer-mediated inflammatory bowel disease. Biochem Biophys Res Communications. 2017 Dec 9;494(1-2):188-193.

2. Muraki Y, Yamasaki M, Takeuchi H, Tohyama K, Sano N, Matsuo T.
Fluorescent Imaging Analysis for Distribution of Fluorescent Dye Labeled- or Encapsulated-Liposome in Monocrotaline-Induced Pulmonary Hypertension Model Rat. Chem. Pharm. Bull. 2018 Mar 1:66(3):270-276.

# Chapter 1 Introduction

## 1.1 Inflammatory bowel disease (IBD) and the environment

Thus far, there is no definitive cause determined for the development of IBD. However, numerous studies suggested that several factors (i.e., food, smoking, and gut microbiota) are involved in disease progression (Figure 1.1) [1].

Previous research demonstrated that the Western food pattern may worsen the state of digestive tract inflammation[2]. For instance, the Western food pattern contains large amounts of refined sugar, omega-6 polyunsaturated fatty acids (PUFAs) and fast foods, combined with deficiencies in fruit, vegetables, and fiber [2] . These Western food patterns are associated with a serious risk to gut health, namely the provocation of the inflammation mediator directory, and dysbiosis of gut microbiota and metabolites in the digestive tract. A previous study suggested that high omega-6/omega-3 PUFA ratios may be related to the development of IBD [3]. Omega-6 fatty acid is a precursor of arachidonic acid and, proinflammatory prostaglandin E2, leukotriene B4, and platelet aggregation thromboxane A2. Unlike omega-6 PUFA, omega-3 PUFA is a precursor of anti-inflammatory prostaglandins E3, which leads to an equilibrium of natural fatty acid ratios to reduce the formation of prostaglandin E2 [3]. Notably, several studies have demonstrated that the Mediterranean food pattern (35% total fat: 15% monounsaturated fatty acids, which are mainly derived from olive oil, 13% saturated fatty acids, and 6% PUFAs) exert a beneficial effect against ulcerative colitis (UC), reduction of inflammatory cytokines, and normalization of the microbiome [4].

In addition, there is increasing evidence regarding the association of smoking and IBD. Surprisingly, the effect against the disease state of IBD is completely different from those against Crohn's disease (CD) and ulcerative colitis: Smoking cessation benefits the improvement of CD, whereas, smoking exerts a protective effect against active UC. The mechanism involved in this process is currently poorly understood.

Studies reported that nicotine, which is an agonist of the aryl hydrocarbon receptor (AhR), has a favorable influence on active UC [5] [6]. Despite the beneficial effect of smoking against active UC, the adverse effects linked to this habit are more serious.

Previous reports demonstrated that exposure to broad-spectrum antibiotics in childhood suppresses the normal development of the microbiome [1]. Finally, recent investigations have stated that gut microbiota homeostasis plays an important role in the function of the gut epithelial barrier and maturation of immune cells. Exposure to antibiotics results in the reduction of particular enterobacteria, causing unusual weight gain and autoimmune diseases, such as inflammatory bowel disease, asthma, allergies, arthritis, and multiple sclerosis [7]. However, several studies highlighted that treatment with antibiotics is effective against pouchitis caused by CD [8].

Collectively, understanding the association between environmental factors and IBD is important in elucidating the etiology and epidemiology of this disorder.

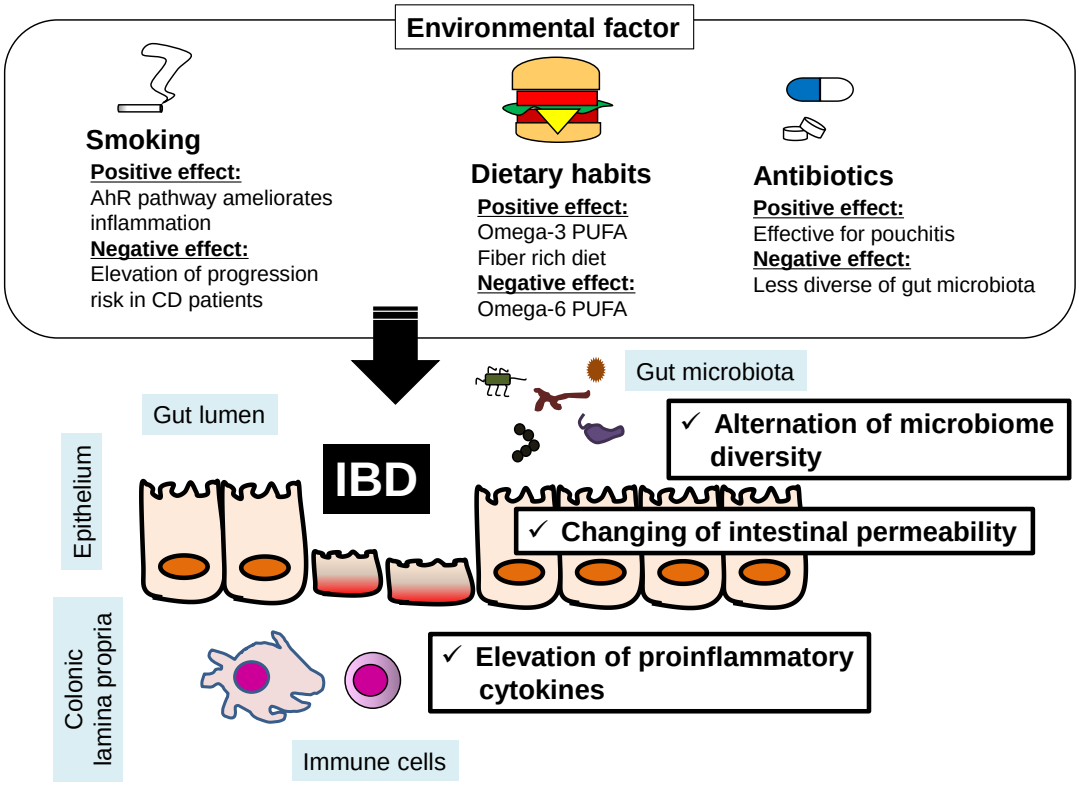


**Figure 1.1 Schematic diagram of how environmental factors contribute to the development of IBD.**

The pathogenesis of inflammatory diseases is deeply influenced by environmental factors, such as alternation of microbiome diversity, changing of intestinal permeability and elevation of proinflammatory cytokines.

## 1.2 The potential of natural products against digestive disorders

It has been proposed that extracts from certain kinds of plants ameliorate digestive disorders[9]. These ingredients possess antioxidant, anti-inflammatory, and anti-cancer properties. For example, polyphenol and flavonoid are extracted from *Oleaceae olea*, and *Lamiaceae Dracocephalum* have a therapeutic effect against IBD. Some plants originating from the Mediterranean or North Africa possess a higher content of these ingredients. These active substances include Oleuropein, Apigenin, Luteolin and Rosmarinic acid. (Figures 1.2 and 1.3) [9]. In Southeast Asia, Indigo naturalis from *Persicaria tinctoria* is used as herbal medicine against UC, improving the function of the mucosal barrier via the IL-22 pathway through activation of AhR. Indigo naturalis includes indigo and indirubin molecules, which act as AhR ligands (Figures 1.2 and 1.3) [6]. In addition, *Prunella vulgaris* contains flavonoids (e.g., rosmarinic acid) and has an anti-inflammatory effect [10]. As mentioned above, these natural products have been widely used for treatment of digestive disorders.

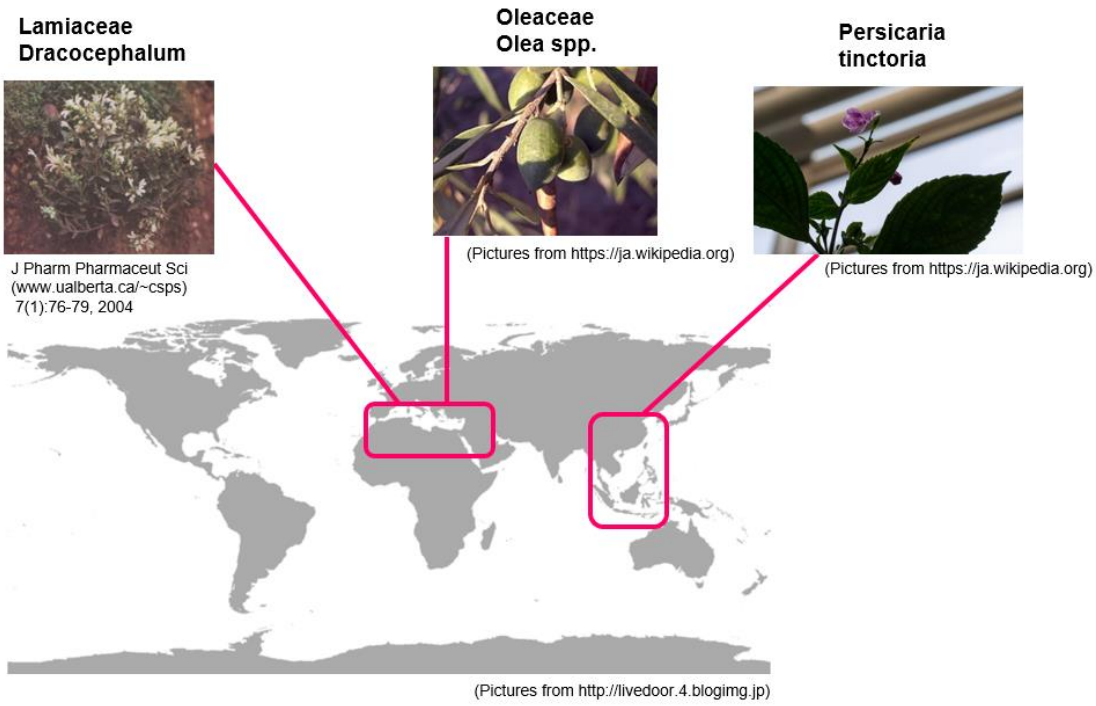


**Figure 1.2 Plants used in the treatment against IBD.**

Extracts from certain kinds of plants ameliorate digestive disorders.

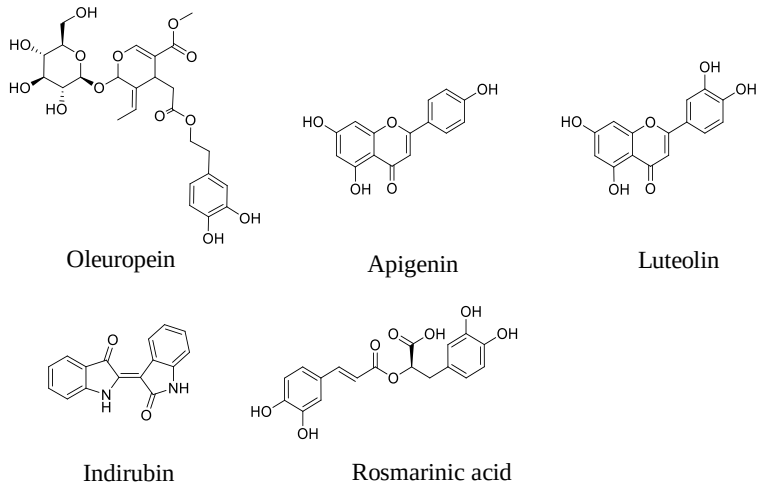


**Figure 1.3 Chemical structures of active substances contained in natural products with therapeutic effects against IBD.**

Oleuropein, apigenin, luteolin, indirubin and rosmarinic acid possess a therapeutic effect against IBD.

### 1.3 Expected benefits of drug delivery systems

The suitable dose of most active pharmaceutical ingredients (APIs) is investigated prior to conducting clinical trials. A drug formulation strategy is required to determine the appropriate dosage. In recent decades, the DDS has been developed. The three major advantages of the DDS are targeting, controlled release, and improvement of absorption. The application of the DDS enhances efficacy, reduces adverse effects, and stabilizes ingredients. Nano- or micro-particle formulation is one of the promising technologies that can encapsulate drug payloads. A wide variety of therapeutic agents can be encapsulated (e.g., compounds, genes, and peptides). Furthermore, size and surface modification of the particle is possible to target specific tissues and cells in the body (Figure 1.4). Following the intravenous administration of particles, large-size particles (~200 nm) tend to accumulate in the spleen and liver, whereas particles <100 nm accumulate in the injury site and/or tumor via a leaky vascular wall with the EPR (enhanced permeability and retention) effect [12]. Moreover, surface modification of the particle realizes more effective delivery to the site of the lesion. In fact, dozens of medicines against cancer and infection that have adapted this technology are currently available. The most commonly used clinical drug formulation is a liposome that consists of lipid bilayers. A major example is liposome-encapsulated doxorubicin, which has been approved as an anticancer drug. Another example is liposomal amphotericin B, which is used against fungal infections. Both drugs have exhibited high efficacy and reduction of adverse effects versus API.

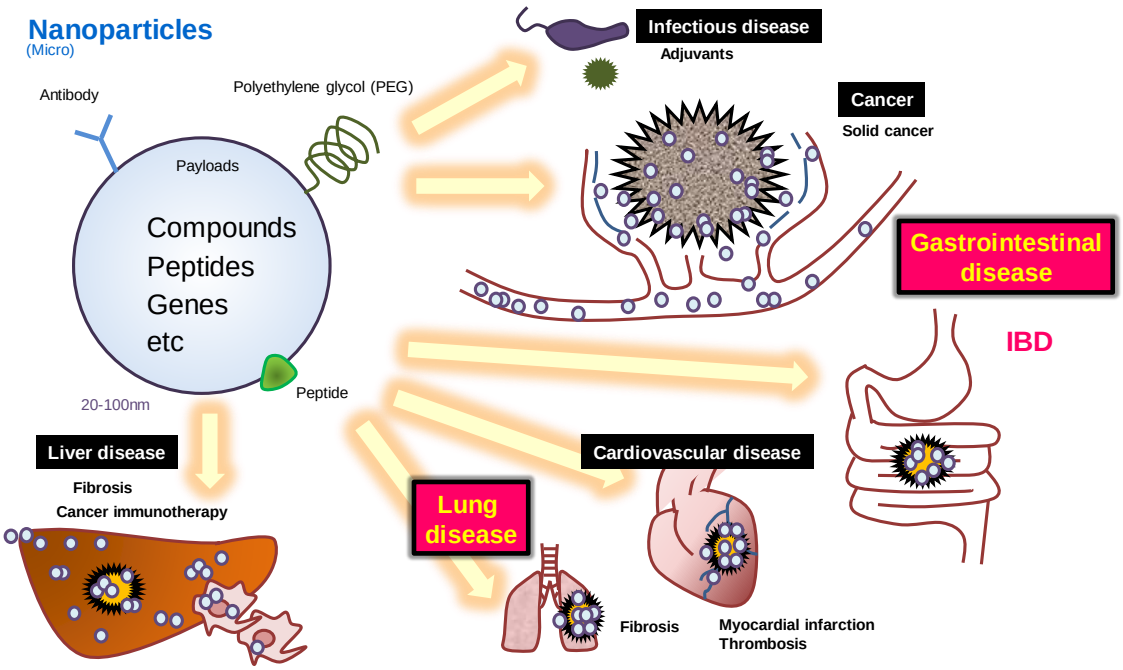


**Figure 1.4 Expected application of drug delivery systems.**

Nano- or micro-particle formulation is one of the promising technologies that can encapsulate drug payloads. A wide variety of therapeutic agents can be encapsulated. Furthermore, size and surface modification of the particle is possible to target specific tissues and cells in the body.

## 1.4 Purpose and contents of this thesis

A formulation strategy is the essential process of drug development. The main purpose of formulation is the realization of "easy to handle," stabilization of payloads, control release, and improvement of absorption. These processes are directly linked to enhancement of efficacy, reduction of adverse effects, and improvement of usage. For example, the leuprorein acetate (a highly active agonist of luteinizing hormone-releasing hormone) deposit formulation is broadly used in clinical practice. Polymer microspheres (20 μm in diameter) encapsulating leuprorein acetate achieve sustained release. Moreover, this formulation strategy is well tolerated for 1–3 months in patients with prostate cancer[13]. In this study, the author investigated nanoparticle delivery to injured tissue and formulation trial for the clinical application of the natural product extract apigenin. The aim was to examine the usefulness of nanosized formulation DDS in terms of targetability and enhancement of the efficacy of natural compounds.

In Chapter 2, the author selected an appropriate liposome to deliver the drug in inflammatory regions using the monocrotaline (MCT)-induced pulmonary hypertension (PH) model—an inflammation model. In Chapter 3, the author evaluated the potential of liposome accumulation in the colitis model. In Chapter 4, the formulation approach of natural products for IBD using the DDS technology was proposed. Furthermore, the possibility for modification of the nanoparticle formulation was also discussed.

# Chapter 2 Verify of the EPR effect in MCT-induced lung injury rat model

## 2.1 Introduction

Natural products are suitable tools for the treatment of inflammatory diseases. For example, treatment with apigenin, which is a plant-derived flavone, improved the symptoms of dextran sulfate sodium-induced colitis in a murine experimental model [11]. However, a limitation of natural products is their short residence in the body. For example, apigenin was removed within few hours after administration to rats [12]. Therefore, appropriate drug carriers are required to develop a treatment method for inflammatory diseases using natural products. To assess the targetability of nanoparticles against inflammatory disease, apart from IBD, the author also focused on the lung injury model. According to the World Health Organization-sponsored 2008 Dana Point Clinical Classification, PH is categorized into the following five groups based on etiologies and histopathological changes: (1) pulmonary arterial hypertension, (2) pulmonary venous hypertension due to left heart disease, (3) pulmonary hypertension due to lung disease/hypoxemia, (4) chronic thromboembolic pulmonary hypertension, and (5) PH due to unclear multifactorial mechanisms [13]. MCT is converted into monocrotaline pyrrole by dehydrogenation of the cytochrome P-450 enzyme in the liver. Subsequently, monocrotaline pyrrole induces damage to pulmonary artery endothelial cells and blood vessels [14]. This rodent model is regarded as a human PH mimicking model because of its similarities to humans in terms of the disease-developing process (i.e., vascular remodeling, proliferation of smooth muscle cells, endothelial dysfunction, upregulation of inflammatory cytokines, and right ventricle failure) [15]. Medications such as phosphodiesterase-5 inhibitors, endothelin receptor antagonists, and prostacyclin analogues are available [13]. However, their therapeutic effects are limited, similarly to the existing medication for the treatment of IBD. One of the potential carriers is liposome, a drug carrier composed of lipid bilayers that can encapsulate natural products. The

residence of drugs in the body and bioavailability of natural products can be improved through encapsulation in liposomes [16].

Size-dependent nanoparticle delivery is an essential element of DDS. The concept of the EPR effect was first reported by Maeda in 1986 [17], demonstrating that the nanosized particles (1–100 nm) passively leak from tumor blood vessels. In general, tumor blood vessels are characterized by immature vessel structure, owing to both tumor vessels having large pore sizes (300–400 nm). Moreover, the lack of a lymphatic system results in the passive accumulation of nanoparticles in the tumor. Abnormal vascularization is observed in tumor vessels and inflammation sites. Thus, high vascular permeability is predicted at these sites, suggesting higher accumulation of nanoparticles. He.C et al. indicated that the size and charge of a nanoparticle can influence the efficiency of its delivery in the tumor [18]. In addition, polyethylene glycol (PEG) coating is a common approach to avoiding aggregation of nanoparticles and the phagocytosis system [19]. In general, large-sized nanoparticles (>200 nm) are easily recognized by the reticuloendothelial system (RES). By contrast, small-sized nanoparticles (<20 nm) are susceptible to elimination through renal clearance. These findings suggested that nanocarrier design should be considered strategically. In Chapter 2, the possibility of site-specific targeting based on the characteristics of the nanoparticle is described.

## 2.2 Materials and methods

### 2.2.1 Preparation of dye-labeled liposomes

FL-labeled liposome was manufactured as reported previously [20]. Liposomes with particle sizes of 80 and 180 nm were prepared using a thin-film hydration method. A mixture of 1,2-distearoyl-sn-glycero-3-phosphocholine (DSPC, NOF Corp., Tokyo, Japan), cholesterol (Chol, WAKO Pure Chemical Industries, Ltd.), and N-(carbonyl-methoxypolyethyleneglycol 5000)-1,2-distearoyl-sn-glycero-3-phosphoethanolamine (DSPE-PEG, NOF Corp.) was dissolved in methanol and ethanol (1:1 v/v) with 1,1′-dioctadecyltetramethyl indotricarbocyanine iodide (DiR, Thermo Fisher Scientific, Inc., MA, USA). The solvent was evaporated to dryness, and the lipid film was further dried overnight. Subsequently, the film was hydrated in a 9% sucrose–water solution to obtain liposomes with a phospholipid concentration of 20 mM. The resultant liposomes were reduced in size through extrusion using a series of polycarbonate membrane filters. Liposomes with a 40 nm particle size were prepared using a microfluidic injection method. A mixture of 1-palmitoyl-2-oleoyl-sn-glycero-3-phosphocholine (POPC, NOF Corp.), Chol, and DSPE-PEG was dissolved in methanol and ethanol (1:1 v/v) with DiR. The dissolved lipids in the organic solvent were subsequently injected into a flow chemistry system (Syrris Ltd., Royston, UK). A 9% sucrose–water solution was also connected to the system. As the organic solvent in the lipid stream diffused and was diluted in the water stream, the lipids tended to assemble into liposomes in a micromixer chip. When the mixture reached equilibrium, stable liposomes were formed. The size distribution and zeta potential of the liposomes were analyzed through a dynamic light scattering method using a Zetasizer Nano analyzer (Malvern Instruments, Ltd., Malvern, UK).

### 2.2.2 Preparation of the MCT model

MCT model was established as reported previously [20]. Male Wistar rats (7-week-old, CLEA Japan, Inc., Tokyo, Japan) were anesthetized using subcutaneously administered isoflurane (3%) and monocrotaline (60 mg/kg, WAKO Pure Chemical Industries, Ltd., Tokyo, Japan) dissolved in saline. The dose of monocrotaline was set to 60 mg/kg because it is generally used to induce pulmonary hypertension within 2 weeks 17). The level of SP-D in the plasma was measured 2 weeks after the administration of monocrotaline using an SP-D enzyme-linked immunosorbent assay kit (Yamasa Corp., Chiba, Japan) to monitor the level of lung injury.

### 2.2.3 Imaging analysis and gene expression analysis

*In vivo* imaging analysis and gene expression analysis was performed as reported previously [20]. DiR-labeled liposomes (30–100 μg/kg DiR) were intravenously administered to the MCT rat model through the tail vein 24 h prior to the measurements. Subsequently, tissue samples were placed into the light-tight chamber of the *in vivo* imaging system (IVIS) Spectrum imaging system (PerkinElmer, Inc., MA, US)and imaged *ex vivo*. The fluorescence intensity of the DiR-labeled liposome in the lung, liver, kidney, and blood was measured at excitation and emission wavelengths of 710 and 760 nm, respectively. For the measurement of vascular permeability, fluorescein isothiocyanate (FITC) albumin (50 mg/kg FITC albumin, Sigma–Aldrich Corp., Inc., MO, USA) was intravenously administered 2 h prior to the measurement. Fluorescence was measured at excitation and emission wavelengths of 465 and 520 nm, respectively. For the measurement of the production of reactive oxygen species (ROS), the luminescent probe 8-amino-5-chloro-7-phenylpyrido[3,4-d]pyridazine-1,4-(2H,3H) dione, L-012 [21] (WAKO Pure Chemical Industries, Ltd.) was intravenously administered at 25 mg/kg

through the tail vein. The lung was isolated and imaged using the IVIS Spectrum *ex vivo* for 3 min. Data acquisition and analysis were performed using the Living Image Software (version 4.4., PerkinElmer, Inc.). The fluorescence and luminescence intensity of the region of interest (ROI) was quantified as average radiant efficiency. Gene expression of CD68 and GAPDH were measured and the Taqman primers/probes Rn01495634_g1 and Rn01775763_g1 (Thermo Fisher Scientific, Inc.) were used, respectively.

### 2.2.4 Data analysis for fluorescent imaging

Data analysis was performed as previously [20]. An analysis of imaging data was performed using the Living Image Software (version 4.4., PerkinElmer, Inc.). Data of the fluorescence and luminescence intensity of the ROI was quantified as average radiant efficiency (p/s/cm²/sr or μW/cm²). The fluorescence of the liver, lung, and blood was normalized to the average fluorescence of the same tissue treated with the 40 nm PEG liposome to evaluate tissue change following accumulation in each tissue according to size and surface modification. Moreover, tissue fluorescence was normalized to that of the same tissue in normal rats to evaluate the change following accumulation of liposome and FITC albumin in the liver, kidney, lung, spleen and blood. Furthermore, the fluorescence of the lung was normalized to that of the lung in normal rats to evaluate the correlation between liposome accumulation in the lung and disease index.

### 2.2.5 Statistical analysis

Statistical analysis was performed as previously [20]. The Student's t-test was used to evaluate differences between two groups. Pearson's correlation coefficient was used to measure the strength of the association between the two groups, and the Bonferroni correction was used for multiple comparisons. p-Values $< 0.05$ were considered statistically significant.

## 2.3 Results

### 2.3.1 Liposome manufacturing

To deliver small molecule compounds to injury sites, the author developed a series of liposomes. The properties of liposomes are summarized in Table 2.1

### 2.3.2 Detection of the inflammation site in the MCT rat model

L-012, a luminescent probe for the detection of ROS (18), was administered to both MCT model and normal rats to detect the inflammatory response in the former. L-012-derived lung luminescence was detected in the MCT model (Figure 2.1A) and increased to 264.9% versus that measured in the normal rats (Figure 2.1B). The level of CD68, one of the markers of macrophage gene expression, was measured in the MCT model. The expression of CD68 in the lung was significantly higher in the MCT model compared with that reported in the normal rats (Figure 2.1.C).

### 2.3.3 Evaluation of liposome accumulation in the lungs of the MCT model

Manufactured liposomes with different compositions and sizes were intravenously injected to MCT model and normal rats to identify the suitable formulation for efficient lung delivery. The fluorescent intensity in the tissue was normalized to the average value of the 40 nm liposome group (the values of the lung, liver, and blood were $2.8 \times 10^8$, $4.3 \times 10^8$, and $3.5 \times 10^7$ [p/s/cm$^2$/sr] / [μW/cm$^2$], respectively). Twenty-four hours after administration, the liposomes did not accumulate in the lung tissue in normal rats. Unlike the 40 and 180 nm liposomes, the 80 nm liposome accumulated in the lung tissues of the MCT model rats. Long retention of all sizes of the PEG and 80 nm liposome was observed in the blood 24 h after administration (Figures 2.2A and 2.2B). Liposomes

with a 40 nm size exhibited higher accumulation in the liver than the 80 nm liposomes (170.5% of the 80 nm liposomes accumulated). Higher accumulation of 180 nm versus 80 nm liposomes was observed in the spleen of injected rats (193.6% of the 80 nm liposomes) in both normal and MCT model rats.

### 2.3.4 Correlation between liposome accumulation and vascular permeability in the lungs

To prove the role of the EPR effect in liposome accumulation in the MCT model, the relationship between vascular permeability and liposome accumulation was investigated using the same rats. The fluorescence value of the 40 nm liposomes and FITC albumin leakage were assessed in the same sample (Figure 2.3A). The tissue fluorescence intensity was normalized to the average value measured in normal rats (the DiR fluorescence in the liver, spleen, kidney, lung, and blood was $1.8 \times 10^8$, $5.3 \times 10^7$, $4.5 \times 10^7$, $8.6 \times 10^7$, and $3.7 \times 10^7$ [p/s/cm$^2$/sr] / [μW/cm$^2$], respectively. The intensity value of FITC fluorescence in the liver, spleen, kidney, lung, and blood was $2.9 \times 10^8$, $5.3 \times 10^7$, $5.2 \times 10^8$, $2.3 \times 10^8$, and $4.1 \times 10^7$ [p/s/cm$^2$/sr] / [μW/cm$^2$], respectively). A higher level of the 40 nm PEG liposomes and significantly elevated vascular permeability were detected in the lungs of the MCT model rats compared with those reported in the normal rats. The accumulation of 40 nm PEG liposomes and FITC albumin was specific to the lung compared with the liver, spleen, kidney, and blood of the MCT model rats (Figure 2.3B and 2.3C). A significant and positive correlation between vascular permeability and the accumulation of 40 nm PEG liposomes was observed (Figure 2.4).

**Table 2.1 Composition and properties of liposomes.**

| Name | Composition | Size (nm) | Fluorescent dye | ζ Potential (mV) |
|---|---|---|---|---|
| 40-nm PEG | POPC/Chol/DSPE–PEG=55/40/5 | 45.3 | DiR | −33.7 |
| 80-nm PEG | DSPC/Chol/DSPE–PEG=50/45/5 | 81.8 | DiR | −48.2 |
| 180-nm PEG | DSPC/Chol/DSPE–PEG=50/45/5 | 178.3 | DiR | −53.5 |
| 40-nm | POPC/Chol/DSPE–PEG=60/40/0 | 36.2 | DiR | 21.5 |
| 80-nm | DSPC/Chol/DSPE–PEG=55/45/0 | 79.6 | DiR | 28.1 |
| 180-nm | DSPC/Chol/DSPE–PEG=55/45/0 | 179.3 | DiR | 25.7 |
| Uranine liposome | DSPC/Chol/DSPE–PEG=68/30/2 | 89.2 | Uranine | −11.9 |

PEG, polyethylene glycol; POPC, 1-palmitoyl-2-oleoyl-sn-glycero-3-phosphocholine; DSPC, 1,2-distearoyl-sn-glycero-3-phosphocholine; Chol, cholesterol; DSPE-PEG, N-(carbonyl-methoxy polyethyleneglycol 5000)-1,2-distearoyl-sn-glycero-3-phosphoethanolamine

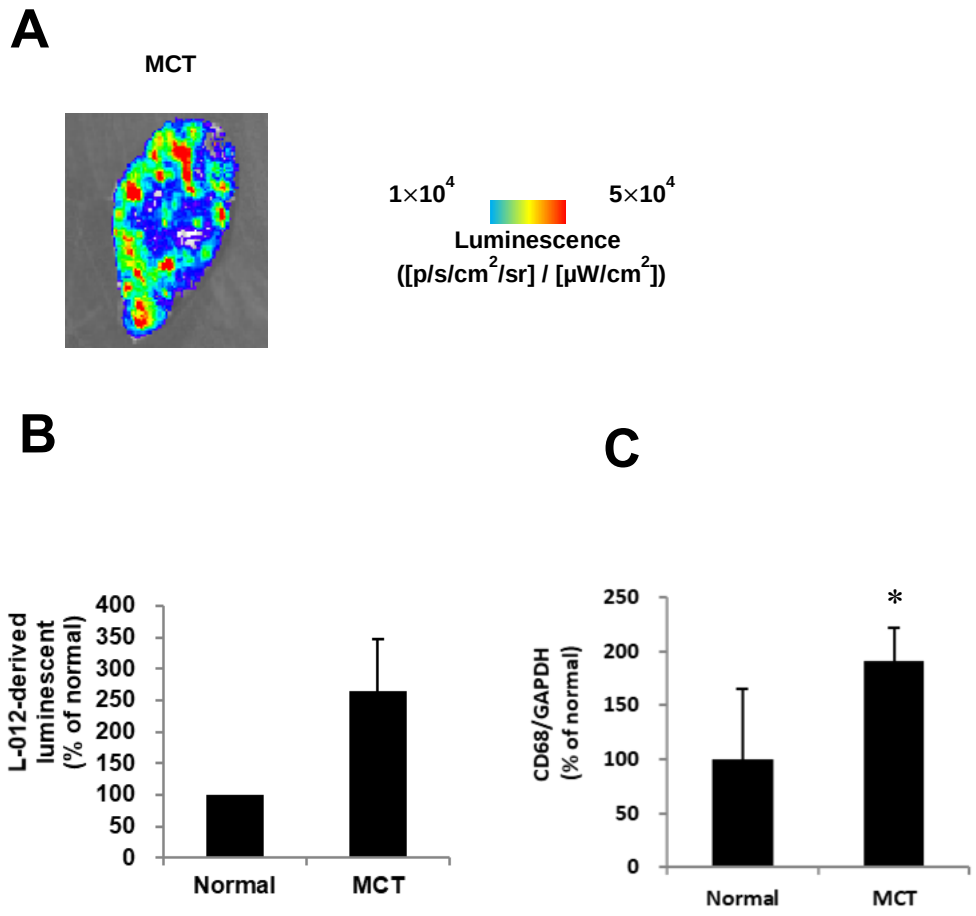


**Figure 2.1 Confirmation of the specific accumulation of FL-labeled liposomes at the lung injury site and relationship between FL-labeled liposome accumulation and macrophage marker in the MCT model.**

L-012-derived luminescent (A) image and (B) signals. L-012 (25 mg/kg) was intravenously administered 1 min prior to measurement (mean + standard deviation (SD), n = 2 and 5 (for normal and MCT groups, respectively)). (C) Expression of cluster of differentiation 68 (CD68) in the lungs of MCT model rats (mean + SD, n = 4 and 9 (normal and MCT groups, respectively)). * $p \leq 0.05$ vs. normal rats using Student's t-test.

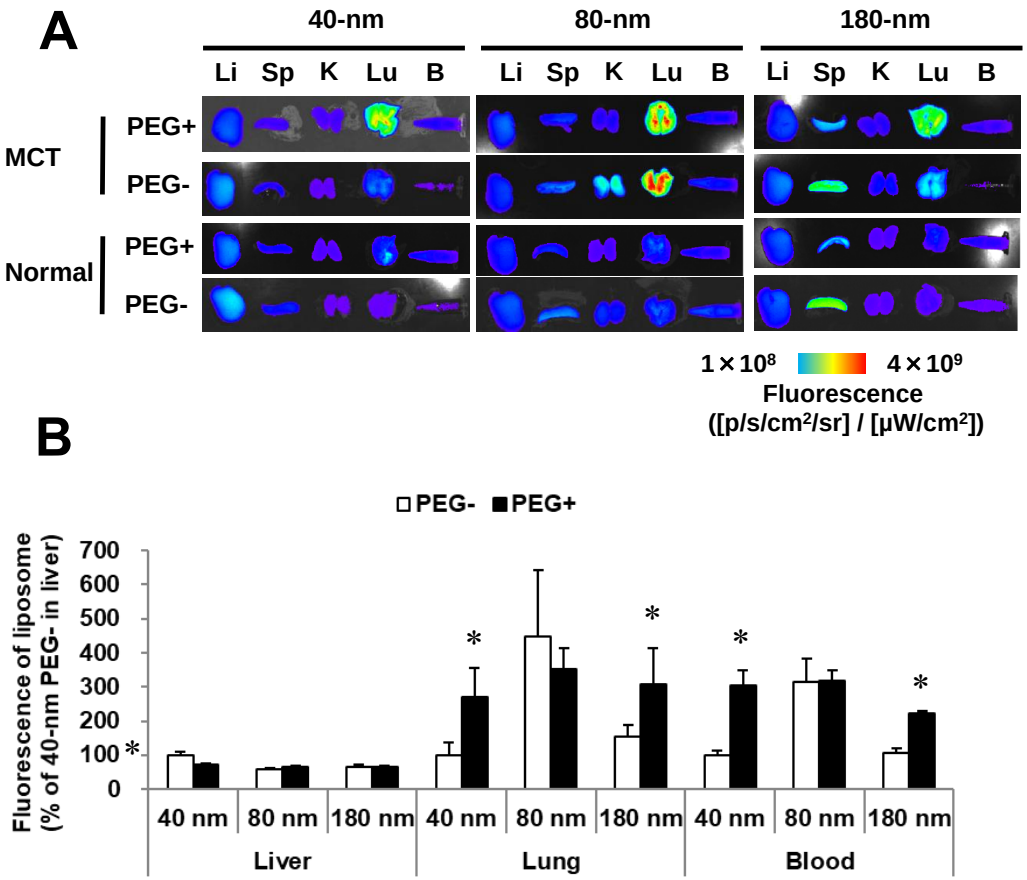


**Figure 2.2 Biodistribution of with/without PEGylated various size FL-labeled liposome Inflammation in the MCT model.**

(A) Fluorescent images of tissues imaged 24 h after the intravenous administration of the DiR liposome (100 μg/kg, DiR) and (B) fluorescence of each tissue in the MCT model (mean + SD, n = 3 or 4 (PEG− or PEG+ groups, respectively). Values were normalized and expressed as a percentage (%) of the 40 nm PEG- group in the liver. *p ≤ 0.05 vs. the PEG− group using Student's t-test.

DiR, 1,1′-dioctadecyltetramethyl indotricarbocyanine iodide; Li, liver; Sp, spleen; K, kidney; Lu, lung; B, blood; MCT, monocrotaline-induced pulmonary hypertension; PEG, polyethylene glycol

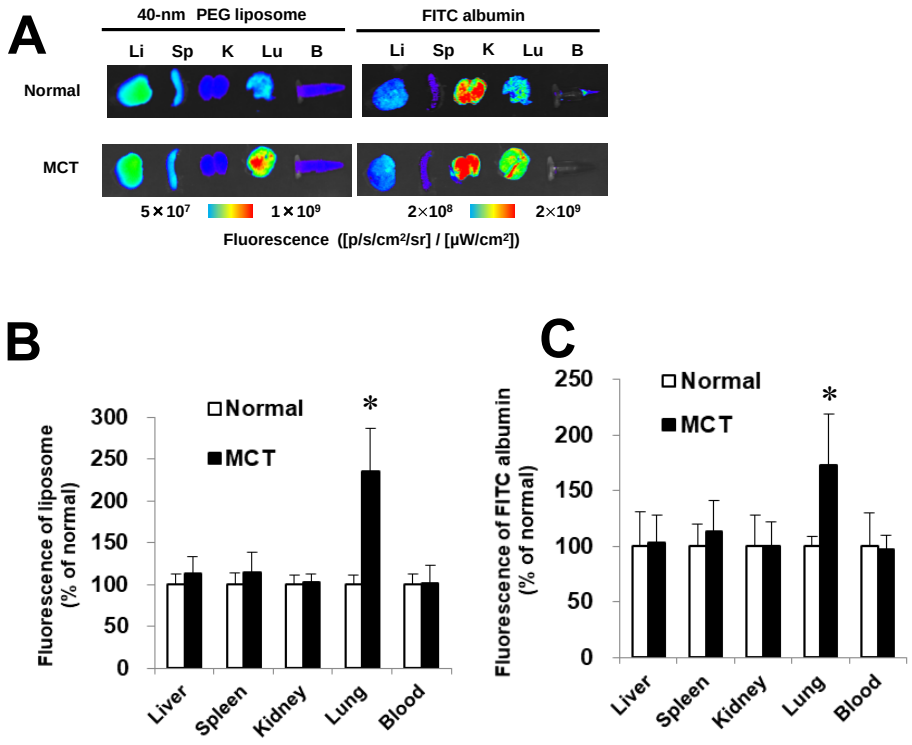


**Figure 2.3 Relationship of vascular permeability and FL-labeled liposome accumulation in the MCT model.**

(A) Fluorescence image of the tissue distribution of 40-nm PEG liposome and FITC albumin in normal and MCT model rats, (B) distribution of DiR liposomes in normal and MCT model rats. DiR liposomes (30 μg/kg, DiR) and FITC albumin (50 mg/kg) were intravenously administered 24 and 2 h prior to measurement, respectively, and (C) vascular permeability in normal and MCT model rats (mean + standard deviation (SD) < n = 4 or 9 (normal or MCT model group, respectively)). Values were normalized to the average values of normal rats. * $p \leq 0.05$ vs. normal rats using Student's t-test. The p-value for the correlation was calculated using Pearson's correlation coefficient. DiR, 1,1′-dioctadecyltetramethyl indotricarbocyanine iodide; Li, liver; Sp, spleen; K, kidney; Lu, lung; B, blood; MCT, monocrotaline-induced pulmonary hypertension model rat; PEG, polyethylene glycol.

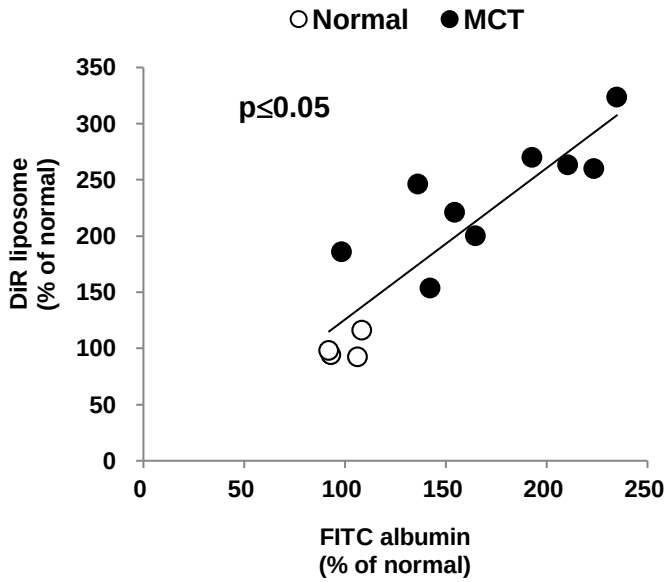


**Figure 2.4 Correlation between the accumulation of 40 nm PEG liposome and vascular permeability in the lungs.**

DiR liposomes (30 μg/kg, DiR) and FITC albumin (50 mg/kg) were intravenously administered 24 and 2 h prior to measurement, respectively. Values were normalized to the average values of normal rats.

## 2.4 Discussion

The results of this study indicated that PEGylated liposome accumulated in the injury site in the MCT model rats through the EPR effect. The author also demonstrated that the accumulation of liposome in the lungs of MCT model rats was significantly and positively correlated to vascular permeability. Enhancement of vascular permeability is an important mechanism for the delivery of liposomes in target tissues. Biodistribution studies of MCT model and normal rats were conducted after the intravenous administration of both FITC albumin and DiR-labeled 40 nm PEG liposome to evaluate the specificity of accumulation at the injury tissue. In comparison with the normal rats, a higher level of the 40 nm PEG liposomes and significantly enhanced vascular permeability were detected in the lungs of the MCT model rats. Conversely, there was no significant difference between the MCT model and normal rats in the other tissues. In addition, vascular permeability was significantly and positively correlated with the accumulation of liposomes. These findings suggest that elevation of vascular permeability is deeply involved in the mechanism of liposome accumulation.

For liposomes without PEG, our results suggest that long residence was achieved based on their size. The 80 nm DSPC-based liposome exhibited long retention in the blood of normal rats without accumulation in the liver and the spleen. In a previous study using normal mice, liposomes were distributed in the blood in a bell-shaped and size-dependent manner. In addition, small-sized (<70 nm) liposomes accumulated in the liver, and an increase in the size of the liposome enhanced its accumulation in the spleen [22]. The liposome with a 110 nm size had long residence in the blood by avoiding accumulation in the liver and the spleen [22]. One of the reasons for the incorporation of the 40 nm liposome in the liver is the pore size in the liver sinus. The estimated pore size of liver sinus was 110 nm [23]. A liposome with a 180 nm size can be retained through

the use of a splenic sinusoidal filter that removes aged red blood cells [24]. A histological study indicated that large-size liposomes accumulated in red pulp, in which meshwork of reticular cell composition [25]. The present results regarding the accumulation of 40 nm and 180 nm liposomes is consistent with the evidence reported in previous studies.

In this study, the author clarified that liposomes with long residence in the blood can accumulate in MCT model rats. Notably, the EPR effect can mediate the accumulation (Figure 2.3). Encapsulation of compounds in the liposome can lower systemic exposure and prolong their residence in target tissue. Focusing on the different lung disorder, these advantages were proved by previous studies. For example, liposomal formulation of amphotericin B for antifungal treatment achieved long circulation in the blood and prolonged the survival time without severe side effects in a mouse model of pulmonary aspergillosis [26] [27]. Therefore, encapsulation of drugs for nanosized liposomes can be a useful drug delivery system for the lungs of patients with PH.

Following the Chapter 2 results, the author evaluated the potential of liposome accumulation in the colitis model and the mechanisms in the Chapter 3.

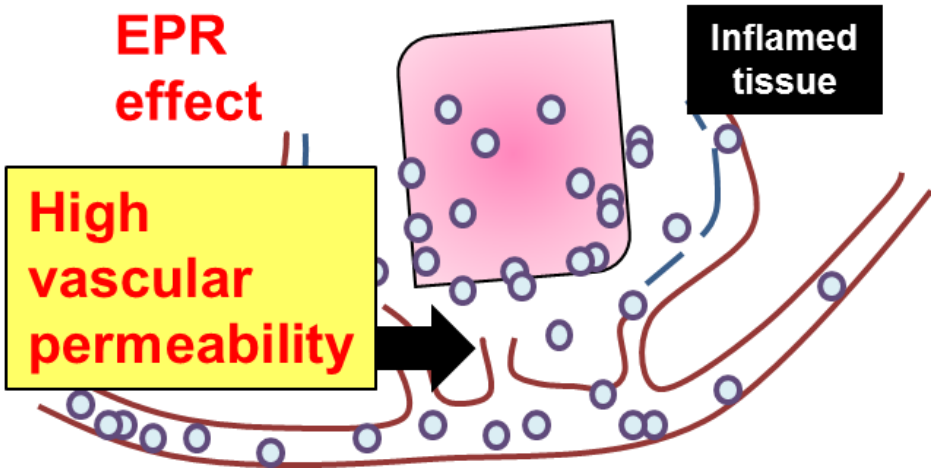


**Figure 2.5 Accumulation of the POPC/DSPC/Chol/DSPE-PEG liposome.**

A liposome can be delivered in inflamed tissue through the EPR effect.

# Chapter 3 Liposome delivery in the inflammatory bowel disease model

## 3.1 Introduction

From the Chapter 2 results, specific accumulation of liposome at the lung injury site through the EPR effects was suggested. In this Chapter, the author evaluated the potential of liposome accumulation in the injury site of colitis model and the mechanisms.

IBD includes CD and UC, whose common symptoms are abdominal pain, diarrhea, and weight loss. The predilection site of CD is any part of the gastrointestinal tract with skipping lesions and cobblestone mucosa, from the mouth to the anus. The cause of IBD is poorly understood. Over 1 million and 2.5 million individuals in the USA and Europe, respectively, are suffering from IBD, which is currently a worldwide health concern [4]. In recent years, various treatment options have become available. However, conventional treatments are characterized by limitations, such as insufficient efficacy and the occurrence of severe adverse effects [28].

Additionally, deep ulcers are observed in CD lesions in the colon walls. By contrast, UC lesions are limited to the large bowel with continuous uniform inflammation, extending only into the mucosa and submucosa. Recent studies suggested that patients with IBD are linked to a risk of developing colorectal cancer, and this risk increases by 0.5–1.0% annually, 8–10 years after diagnosis [29]. A bimodal peak of age at onset is reported in CD: the 20–30-year age group and the 60–70-year age group. Meanwhile, the peak incidence age for UC is 20–30 years [30]. IBD exhibits the highest prevalence in North America (UC: 286 per 100,000 in the USA, CD: 319 per 100,000 in Canada) and Europe (UC: 505 per 100,000 in Norway, CD: 322 per 100,000 in Germany); conversely, it is less common in Asia [31]. It is presumed that the incidence rate of IBD tends to be higher in developing countries [31], with some studies suggesting that the “urban environment” is involved in the onset of IBD [2].

The main function of the digestive tract is the digestion of food and absorption of nutrients. However, recent studies emphasized their importance in the immune system. In other words, immune cells derived from gut immune organs, such as Peyer's patches and mesenteric lymph nodes, may be key players in the development of the immune system for the whole body [32]. In particular, immune cells at the intestinal epithelial barrier play a crucial role in the maintenance of gut environmental homeostasis [32]. The intestinal mucosal barrier involves a biological defense mechanism, which is regulated by mucosal immune cells against gut bacteria. Dendritic cells, macrophages and T cells are stimulated by over tens of thousands of gut bacteria [33]. These cells protect from bacterial invasion. In addition, antimicrobial peptides are secreted by intestinal epithelial cells. It is essential to undergo this process since infancy; microbiome diversity is associated with the development of the immune system [34]. However, the lack of microbiome diversity (i.e., dysbiosis) provokes imbalance of the intestinal environment [34]. The latest reports suggest that a wide variety of diseases (e.g., IBD, obesity, diabetes, depression, cancer, and allergy) are related to the gut microbiota [35]. In fact, dysbiosis links with host's condition deeply. Regarding IBD, overreaction of immune cells against gut bacteria and breakdown of the gut epithelial barrier are suspected causes of inflammation. Regulatory T cells are known as a modulator of the activated effector immune cells. Specifically, it has been reported that microbial metabolites, such as short chain fatty acids (acetic acid, propionic acid and butyric acid) produced by *Bacteroides spp.* promote the production of IL-10 and enhance the function of regulatory T cells. However, dysbiosis decreases *Bacteroides spp.* and migrates over to another bacterium dominant environment [36]. The host innate defense mechanism is important for maintaining intestinal epithelial barrier homeostasis. NOD-like receptor family pyrin containing (Nlrp) forms an inflammasome complex with an apoptosis-associated speck-

like protein containing a caspase recruitment domain and caspase-1, which promotes inflammatory response against pathogens at the mucosal barrier [37]. Activation of the inflammasome leads to the production of IL-18, IL-1b, and anti-microbials and defends the mucosal barrier against an invasion of gut microbacteria. This cycle is necessary for the development of the immune system in the mucosal barrier, and deficiencies in this cycle are related to the development of IBD.

Therapeutic approaches against CD and UC are similar. Mesalazine (5-aminosalicylic acid, 5-ASA) is currently the primary option for the treatment of these conditions. Some studies suggested that Mesalazine has the anti-oxidant and inhibitory effects of leukotrieneB4 [38]. In case of moderate inflammation, a synthetic adrenocortical hormone, such as prednisolone, is prescribed to the patients. For patients with advanced or refractory symptoms, biological products against IBD, such as adalimumab or infliximab, are selected. The pharmacological effects of these products is that they are known as monoclonal antibodies against TNF-α. In addition, the United States Food and Drug Administration-approved vedolizumab reacts with integrin α4β7 (lymphocyte Peyer's patch adhesion molecule 1) and inhibits adhesion of the immune cells to the colon wall. As a last resort in the treatment of IBD, colectomy has been widely applied to patients with severe IBD. The latest therapeutic approach for patients with complex perianal fistula is stem cell therapy. Implantation of adipose-derived stem cells (Cx601) achieved clinical remission in a phase 3 trial. It is expected that Cx601 will be an alternative treatment to surgery. In the previous decades, transplantation of fecal microbiota has been investigated as a new safe treatment for IBD. The United States Food and Drug Administration approved this treatment against refractory infection with *Clostridium difficile* in 2013 [39]. Changing the diversity of the gut microbiome renders the improvement of the host intestinal environment possible. Thus, this method can also

be adopted for the treatment of IBD. Several meta-analyses and cohort studies have exhibited the efficacy of microbiota transplantation [39].

In terms of adverse effects, 5-ASA drugs are safer than other types of drugs against IBD. However, allergic reactions were observed in 5%–10% of patients [28], and it is difficult to maintain complete remission after inflammatory recurrence. Regarding the efficacy of corticosteroids, 16% of patients were not cured, and 20%–30% had only a limited response [28]. In addition, long-term treatment with corticosteroids causes severe adverse effects. Therapy with anti-TNF-α drugs is a promising treatment option. However, anti-TNF-α drugs are costly and associated with the risk of carcinogenicity [28]. Considering efficacy, adverse effects and cost, there are several limitations in biological drug treatment; novel therapeutic indications for IBD are desired; and innovative medicines are warranted. As outlined above, IBD is affected by environmental factors, such as smoking, food, and the microbiome. Advanced therapies for IBD require a therapeutic strategy taking into consideration the environmental factors. In addition, the development of more target-specific treatments and concomitant use of several IBD medicines are necessary. The use of nanoparticles is one of the attractive DDSs to maximize efficacy and reduce the incidence of adverse effects. These formulations can improve the pharmacokinetic profiles and pharmacodynamic effects and reduce adverse effects.

The author explored whether liposomal formulations can specifically accumulate at the injury site of the colon and clarified the role of macrophages with liposomal uptake to determine the specific targetability of DDS.

## 3.2 Materials and methods

### 3.2.1 Concanavalin A (ConA)-activated T-cell transfer IBD mouse model

Con-A-activated T cell transfer IBD model was established as reported previously[40].

**Animals**

Female, 6-week-old BALB/cAnNCrlCrlj (BALB/c) mice were purchased from Charles River Laboratories Japan (Tokyo, Japan).

**Implantation**

Lymphocytes were isolated from spleens of 7–9-week-old female BALB/c mice and incubated in a $2 \times 10^6$ cells/75 $cm^2$ flask in a Roswell Park Memorial Institute 1640 medium (Invitrogen, US) supplemented with 10% fetal bovine serum containing 1 μg/mL ConA (WAKO Pure Chemicals Industries, Japan) and 10 ng/mL interleukin (IL)-2 (R&D Systems, MN, USA) in an atmosphere of 95% air and 5% $CO_2$ at 37°C for 72 h. $CD4^+$ T cells were isolated from the incubated lymphocytes using the MACS $CD4^+$ T-cell isolation kit (Miltenyi Biotec, Bergisch Gladbach, Germany) and intravenously transferred into recipient 6–8-week-old female C.B17/Icr-scid/scid Jcl (severe combined immunodeficiency [SCID]) mice (CLEA Japan, Inc.). Untreated SCID mice served as the controls.

**Follow-up**

The development of colitis in SCID mice was followed by monitoring of stool consistency, and the diarrhea score was blindly recorded. The severity of diarrhea was scored using the following scale: 0 (untreated), 1 (normal), 2 (pasty and formed), 3 (pasty and unformed), and 4 (diarrhea). All mice were fed a standard diet (CE-2, CLEA Japan, Inc.) and had *ad libitum* access to drinking water. All experiments were approved by the Institutional Animal Care and Use Committee of Shonan Research Center, Takeda Pharmaceutical Company, Ltd.

### 3.2.2 FL (fluorescent)-labeled liposomes

**Nanoparticle formulation**

FL-labeled liposome was manufactured as reported previously[40]. Liposomes labeled with 1,1'-dioctadecyl-3,3,3',3'-tetramethylindotricarbocyanine iodide consisting of L-α-distearoyl- phosphatidylcholine (DSPC):cholesterol:polyethylene glycol PEG 5000-L-α-distearoyl-phosphatidylethanolamine (DSPE):DiR = 50:45:5:0.5 (mol%) were manufactured using the extruder method. Free DiR was dispersed into a 9% sucrose solution and served as the control. The concentration of DiR was evaluated using a microplate reader (Molecular Devices, excitation: 748 nm, emission: 780 nm). The particles size was approximately 100 nm, measured using dynamic light scattering (Malvern). All formulations were manufactured at the Pharmaceutical Sciences Formulation Development of Takeda Pharmaceutical Company, Ltd. (Osaka, Japan).

### 3.2.3 *In vivo* imaging analysis

**Fluorescence image**

*In vivo* imaging analysis was performed as reported previously[40]. Twenty-six days after implantation, free DiR- (3 μg) or DiR-labeled (3 μg DiR equivalent) liposome was intravenously administered to the mice, and the diarrhea score was recorded. Prior to the FL imaging study, the mice were fasted for 18 h. Twenty-four hours after administration, the mice were euthanized, and whole blood samples were collected from the heart under anesthesia with isoflurane. Subsequently, the organs of each mouse were removed, and the colon tissues were weighed. The average radiant efficiency [p/s/cm²/sr]/[μW/cm²] was measured and calculated using the *in vivo* imaging system (IVIS) spectrum (PerkinElmer, USA) and the Living Image® software to evaluate the accumulation of FL-labeled liposomes.

### 3.2.4 Detection of ROS in the mouse colitis model

**Luminescence image**

Twenty-eight days after implantation, L-012 (WAKO, Japan), a luminol-based chemiluminescent probe (20 mg/kg) for the detection of ROS, was intravenously administered to each mouse, and the diarrhea score was recorded. Five minutes after administration, the average radiance efficiency [p/s/cm²/sr] was measured under anesthesia with isoflurane and calculated using the IVIS spectrum and the Living Image® software**.**

### 3.2.5 Confirmation of specific accumulation of FL-labeled liposomes at the injury site Dual fluorescence/luminescence image

Thirty days after implantation, DiR-labeled liposomes (3 μg DiR equivalent) were intravenously administered to untreated (score 0) and treated (score 4) mice. Twenty-four hours after administration, L-012 (WAKO, Japan), a luminol-based chemiluminescent probe (20 mg/kg) was intravenously administered to each mouse, and the diarrhea score was recorded. Five minutes after administration, the luminescence and fluorescence were measured and calculated using the IVIS spectrum *in-vivo* imaging system and the Living Image® software.

### 3.2.6 Macrophage marker gene expression analysis in the colon

**Real-time PCR**

Gene expression analysis was performed as reported previously[40]. Colon tissues were lyzed in the lysis buffer provided in the RNeasy mini kit (Qiagen, Germany). Total RNA was purified using the RNeasy mini kit according to the manufacturer's instructions. Complimentary DNA was synthesized using reverse transcription (RT,

SuperScript® VILO™ cDNA synthesis kit, Life Technologies, USA) using isolated total RNA as a template. The levels of mRNA expression were measured through a quantitative real-time RT-polymerase chain reaction using the qPCR MASTER MIX (Nippon Gene, Japan) and ABI 7900HT (Life Technologies, USA). The target mRNA-specific primer and probe sets are listed in Table 1. Each mRNA expression was calculated using the ΔΔCt method according to the manufacturer's instructions, and the mRNA expression levels of CD68, CD204, and F4/80 were normalized to those of hypoxanthine-guanine phosphoribosyltransferase (HPRT) (internal control) (Table 3.1).

### 3.2.7 Statistical analysis

**Statistical significance test**

Stastistical analysis was performed as reported previously[40]. For comparisons between three or more groups, a one-tailed Williams test or a two-tailed Shirley–Williams test was used. p-Values < 0.025 were considered statistically significant. The Spearman correlation coefficient was used to analyze the correlation between two groups. Statistical differences between two groups with p-values < 0.05 were considered significant.

## 3.3 Results

### 3.3.1 Confirmation of the specific accumulation of FL-labeled liposomes at the colon tissue in the mouse colitis model

The author investigated the biodistribution of fluorescent-labeled liposomes after intravenous administration in a T-cell transfer mouse model of colitis to determine the advantages of DDS in IBD. The T-cell transfer model is a more important model of chronic colitis mediated by T cells, such as TH17, TH1, and regulatory T cells, compared with other mouse colitis models (Table 3.2) [41] [42]. Colon-wall thickening and elongation by swelling are observed in a colitis-severity-dependent manner (Figure 3.1). DiR was selected as the FL reagent. This reagent allows imaging with minimal intrinsic fluorescence owing to its longer excitation and emission wavelength. In addition, DiR can be combined with the lipid component of the liposome membrane owing to its hydrophobic property. Initially, the author evaluated the accumulation of FL-labeled liposomes in various disease states using IVIS. The results indicated that DiR-labeled liposomes accumulated in a colitis-score-dependent manner, although the DiR solution did not accumulate even in tissues of mice with severe colitis (Figures 3.2 and 3.3). In addition, the levels of fluorescence intensity were correlated with the colon weight and diarrhea score (Figures 3.4 and 3.5).

### 3.3.2 Biodistribution analysis by IVIS

Strauch et al. reported that induction of colitis in germ-free mice did not result in disease progression [43]. Therefore, it is suggested that commensal gut bacteria function as antigens in this model; as can be seen from this model characteristic, localized inflammation in the colon tissue is assumed. The author assessed other organs (including the colon) in the mouse colitis model to confirm the biodistribution of the FL-labeled

liposomes in the whole body. The accumulation of the FL-labeled liposome in the inflamed colon was more specific compared with that observed in the other organs (Figure 3.6).

### 3.3.3 Simultaneous imaging of inflammation site detection and FL-labeled liposome accumulation

Subsequently, the colon injury site of mice with colitis was imaged by IVIS using L-012, a luminol-based chemiluminescent probe for the detection of ROS. L-012 can visualize sites of tissue injury, because elevation of immune-cell-derived production of ROS is observed in inflammation. The results of *in vivo* living imaging indicated that levels of luminescence intensity were significantly increased in mice with colitis versus normal mice (Figures 3.7 and 3.8). Furthermore, the lesion site in the colon tissue approximately corresponded to the accumulation of FL-labeled liposomes (Figure 3.9). Thus, the levels of luminescence intensity correlated with the accumulation FL-labeled liposomes (Figure 3.10).

### 3.3.4 Identification of macrophage cellular uptake

Finally, the cells that uptake FL-liposomes were determined. In general, intravenously administered nanoparticles are taken up by the reticuloendothelial system. Therefore, the gene expression levels of three macrophage markers (i.e., CD68, CD204, and F4/80) were examined in colon tissues of mice at various disease states. All macrophage gene markers correlated with the accumulation of FL-labeled liposomes. These results suggested that FL liposomes may be efficiently delivered to macrophages (Figure 3.11).

In addition, the results suggested that FL-labeled liposomes specifically accumulate to the injury site of the colon. Hence, this technology may be a novel attractive strategy for the development of drugs, such as macrophage-targeting drugs, against IBD.

**Table 3.1 Three major types of mouse colitis models.**

| Model | Inducer | Route | Evaluation target | Mechanism of colitis induction |
|---|---|---|---|---|
| **DSS induced colitis** | Dextran sulphate sodium | Oral | Epithelial barrier function | DSS is one of mucopolysaccharide, it provokes epithelial cell tight junction damage with chelation of divalent cation(Mg+ and Ca+), followed by invasion of proinflammatory intestinal contents (e.g. bacteria and their products) into lamina propiria mucosae |
| **TBNS induced colitis** | 2,4,6-trinitrobenzene sulfonic acid | Intrarectal | Efficacy of anti-cytokine therapies | Rectal administration of the hapten reagent TNBS induces immunogenic reactions of CD 4+ T cell, macrophages, and neutrophil in the colon wall |
| **Cell transfer induced colitis** | Lymphocytes transplantation | Intravenously | Immunoregulation and regulatory T cells | Naive T cell transfer model is defined one of the important model of chronic colitis mediated by T cells such as TH17, TH1and regulatory T cells |

Current experimental colitis animal models depend on pathological characteristics

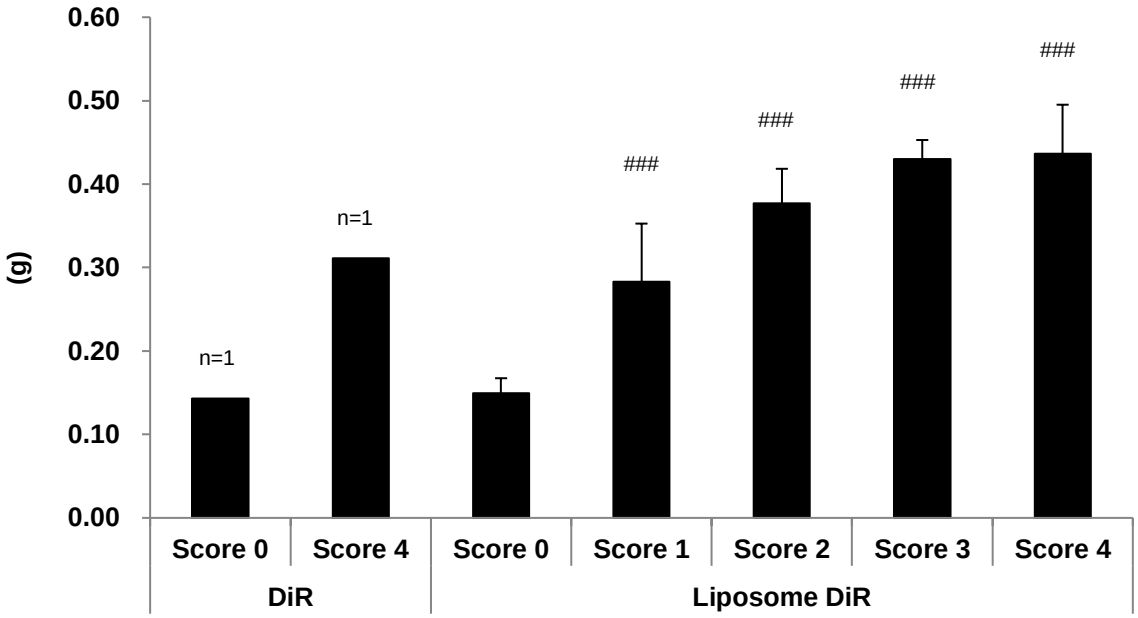


**Figure 3.1 Quantification of the weight of mouse colon tissues in the colon tissue of mice with IBD at various disease states.**

A statistical analysis was performed between the DiR-labeled and liposome-treated mouse groups. Data are expressed as mean ± SD (n = 5), ### $p < 0.0005$ by one-tailed Williams test.

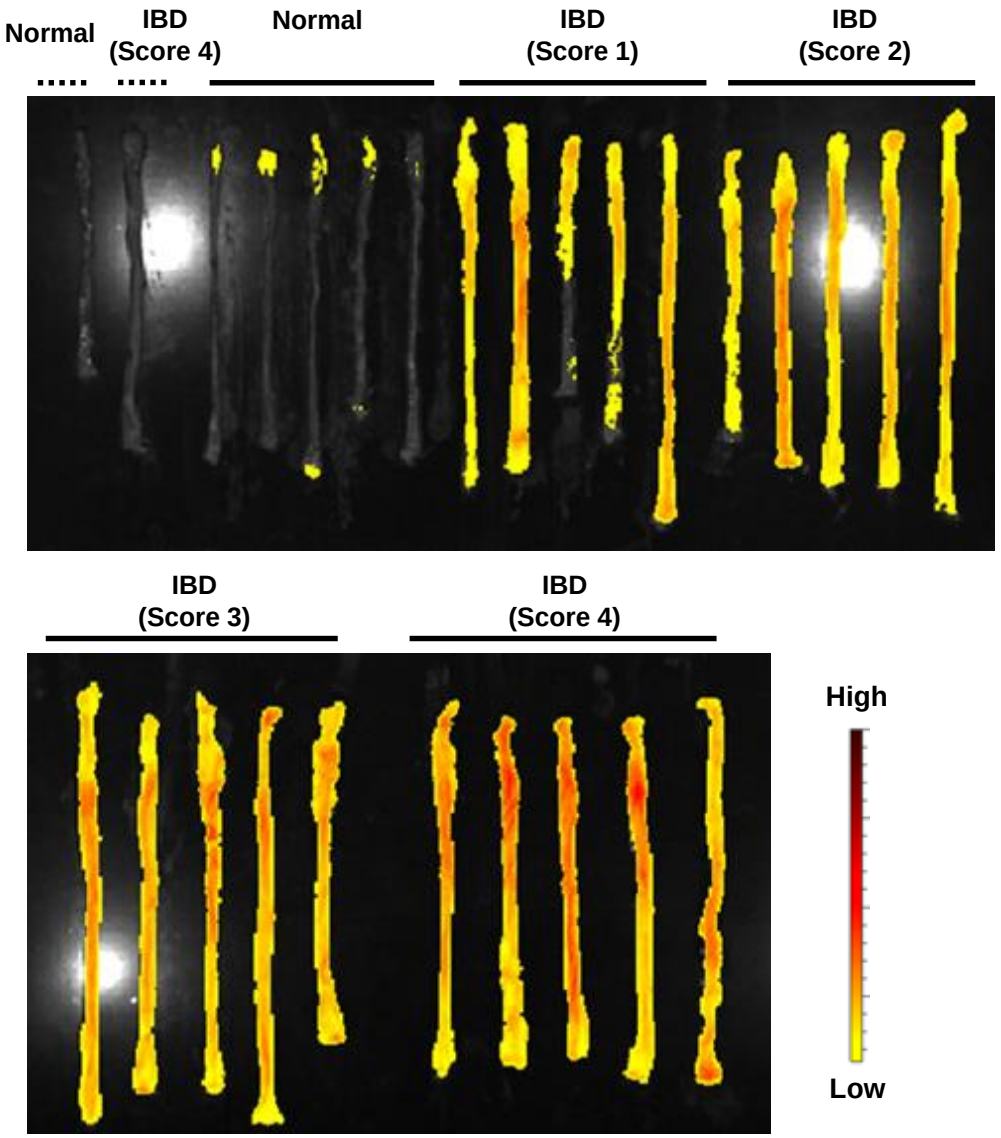


**Figure 3.2 Quantification of the weight of mice colon tissues in the colon tissue of mice with IBD at various disease states.**

Biodistribution analysis of the DiR solution- or DiR-labeled liposomes by IVIS imaging in the colon tissue of mice with IBD at various disease states. DiR solution-treated mice (dotted lines, n = 1) and DiR-labeled liposome-treated mice (solid line, n = 5).

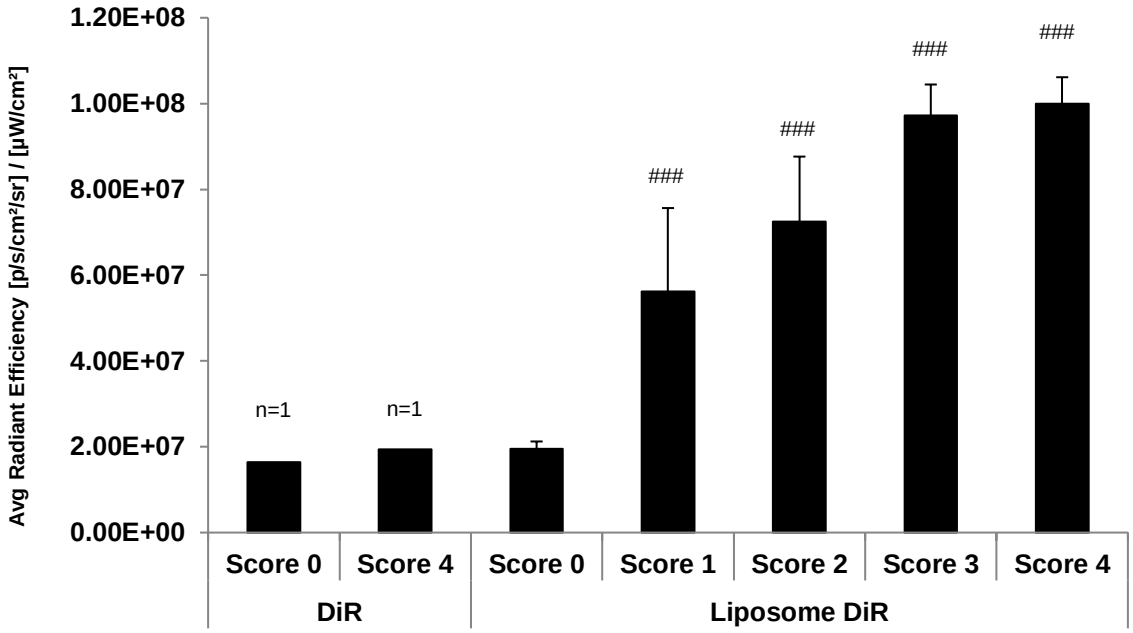


**Figure 3.3 Quantification of luminescence intensity in the colon tissue of mice with IBD at various disease states.**

A statistical analysis was performed between the DiR-labeled and liposome-treated mouse groups. Data are expressed as mean ± SD (n = 5). ### $p < 0.0005$ by one-tailed Williams test.

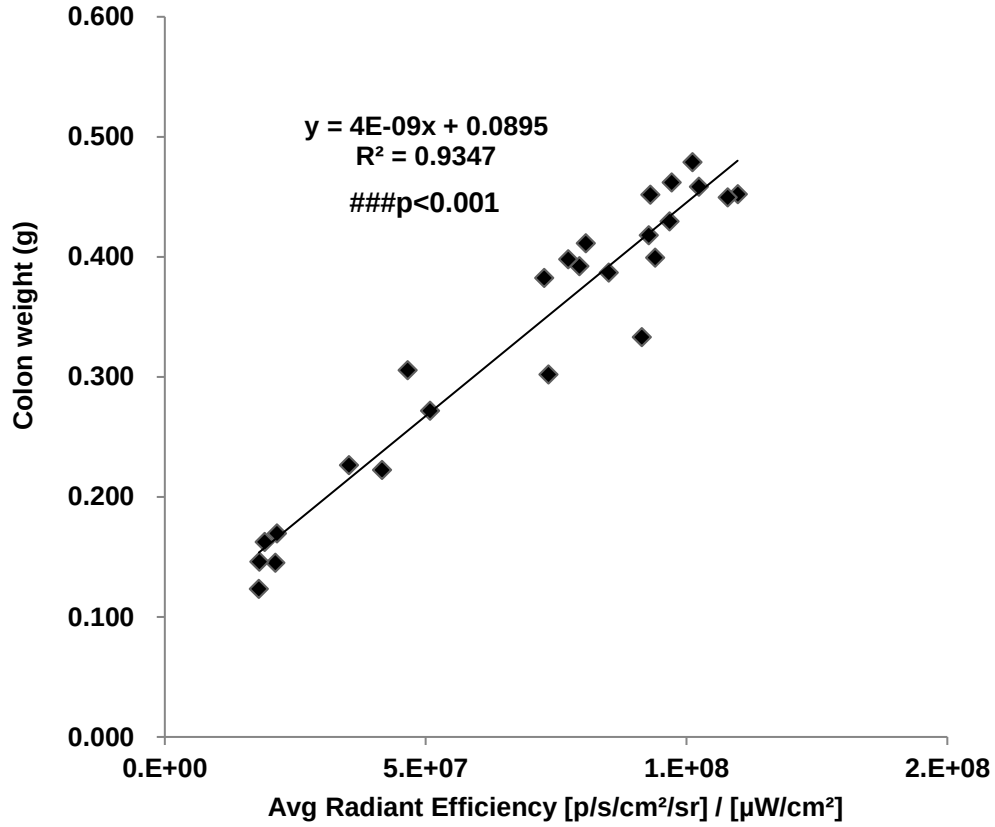


**Figure 3.4 Correlation between tissue weight and fluorescence intensity in the colon tissues of mice at various disease states.**

A statistical analysis was performed between the DiR-labeled and liposome-treated score 0–4 mice groups (n = 5 each). ### $p < 0.001$ by Spearman correlation.

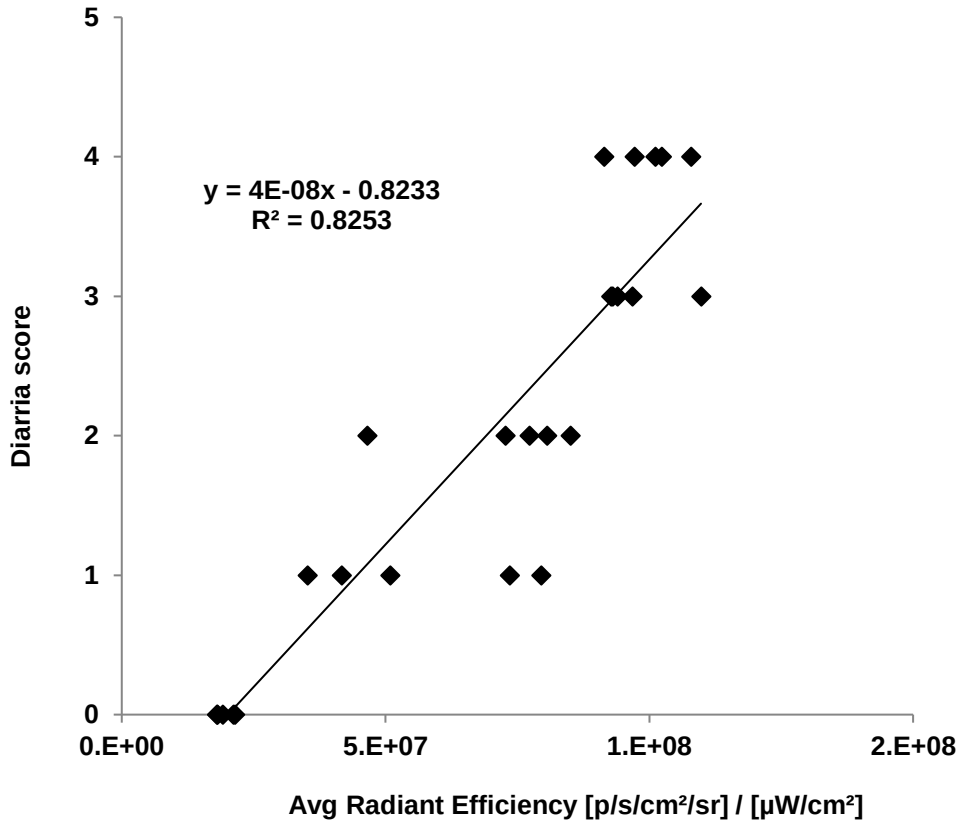


**Figure 3.5 Correlation between the diarrhea score and fluorescence intensity in the colon tissues of mice at various disease states.**

A statistical analysis was performed between the DiR-labeled and liposome-treated score 0–4 mouse groups (n = 5 each). ### $p < 0.001$ by Spearman correlation.

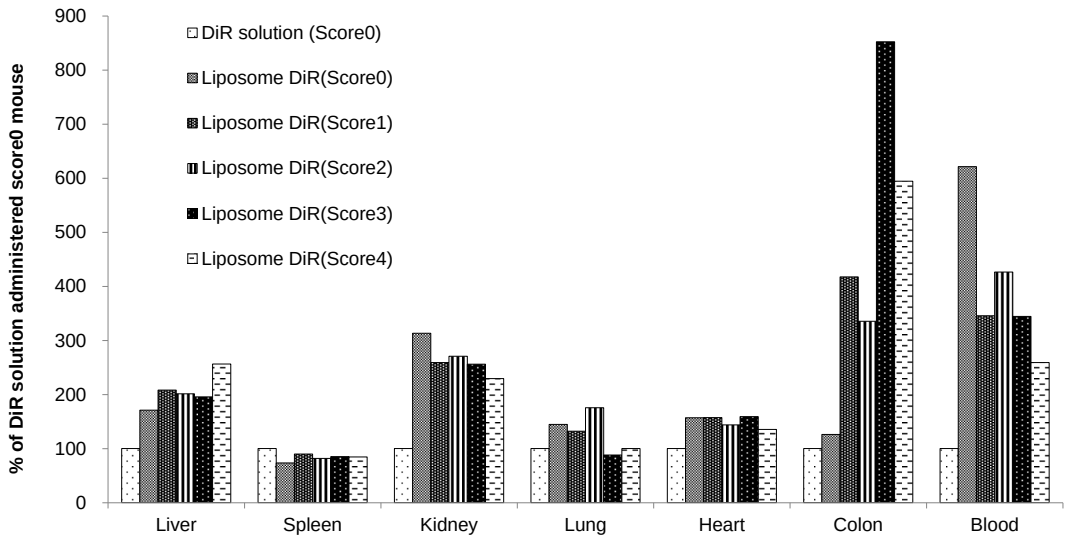


**Figure 3.6 Assessment of the tissue biodistribution of the DiR-labeled liposome in mice with IBD at various disease states.**

Fluorescence in each tissue of score 0 mice treated with the DiR solution was defined as 100% (n = 1, each).

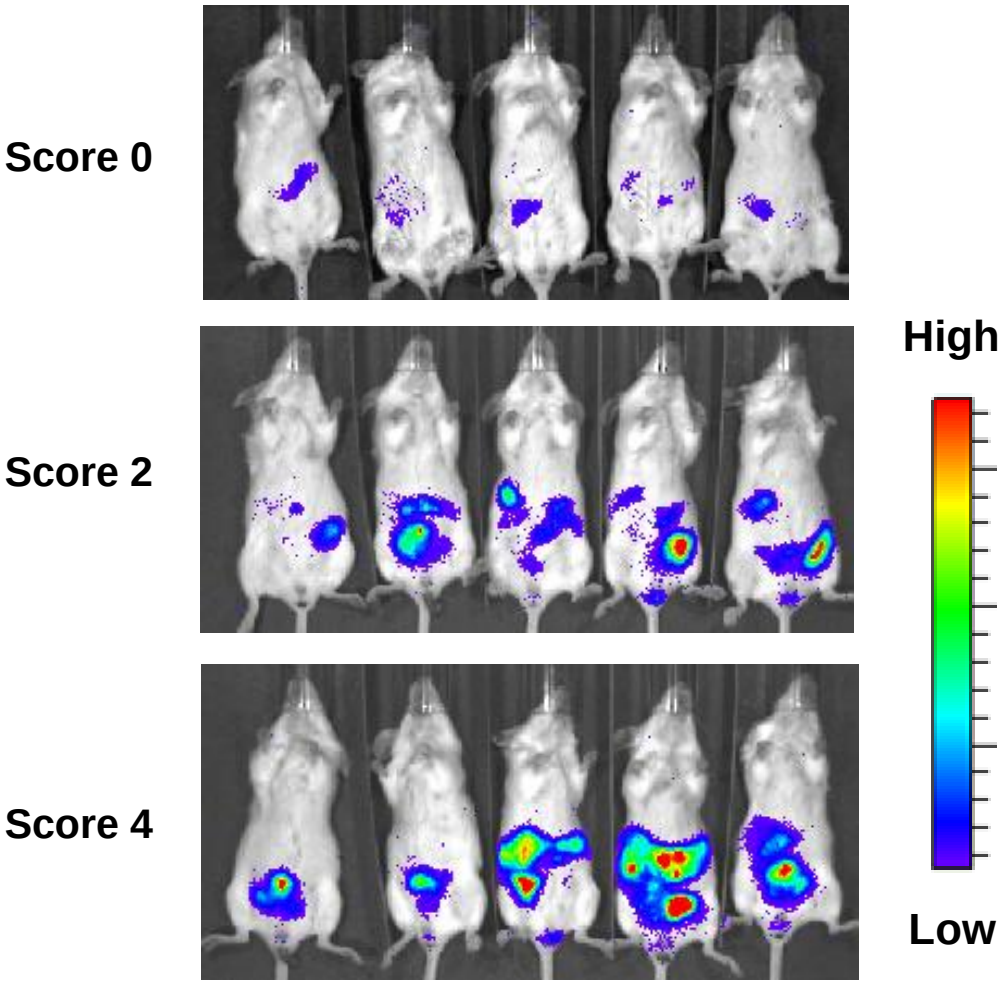


**Figure 3.7 Optical imaging of ROS detection and accumulation of the DiR-labeled liposome in score 0, 2, and 4 mice with IBD.**

A living image of ROS production by IVIS. Data are expressed as mean ± SD (n = 5).

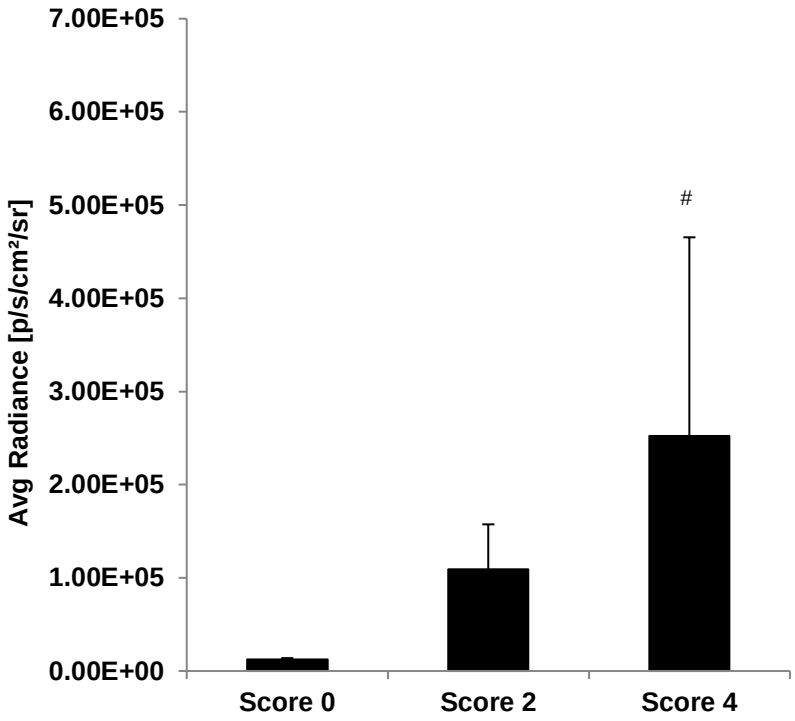


**Figure 3.8 Quantification of luminescence intensity using the IVIS software in score 0, 2 and 4 mice with IBD.**

Data are expressed as mean ± SD (n = 5) # $p < 0.05$ by two-tailed Shirley–Williams test.

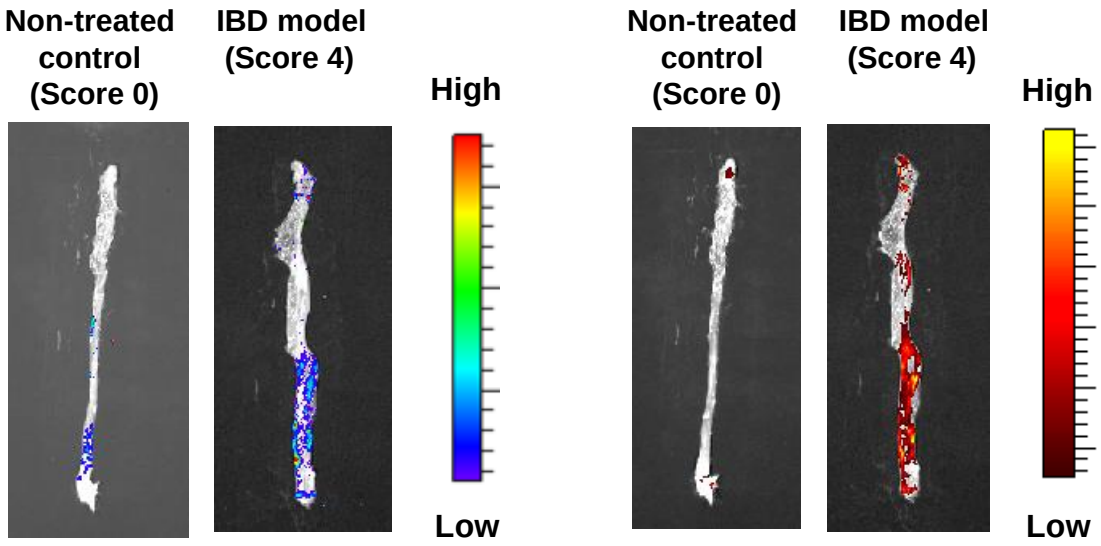


**Figure 3.9 Luminescence for the detection of ROS (left) and fluorescence for DiR (right) images of score 0 versus score 4 mice.**

Data were taken by luminescence or fluorescence setting in IVIS (n = 1, each).

.

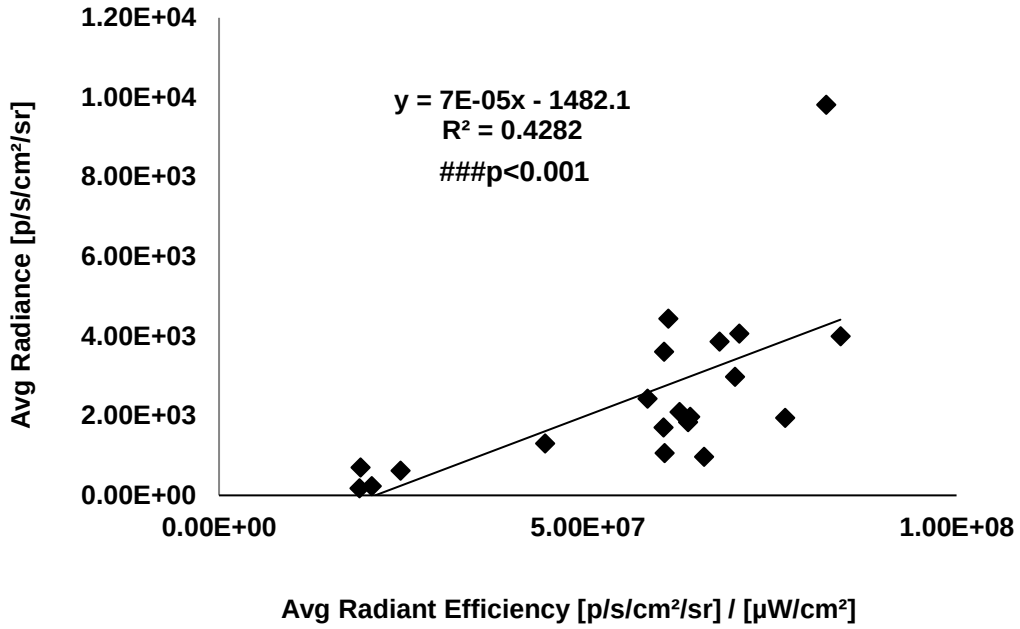


**Figure 3.10 Correlation between the production of ROS and fluorescence intensity in the colon tissues of mice.**

A statistical analysis was performed between the DiR-labeled and liposome-treated score 0–4 mouse groups (n = 4 each). ### $p < 0.001$ by Spearman correlation.

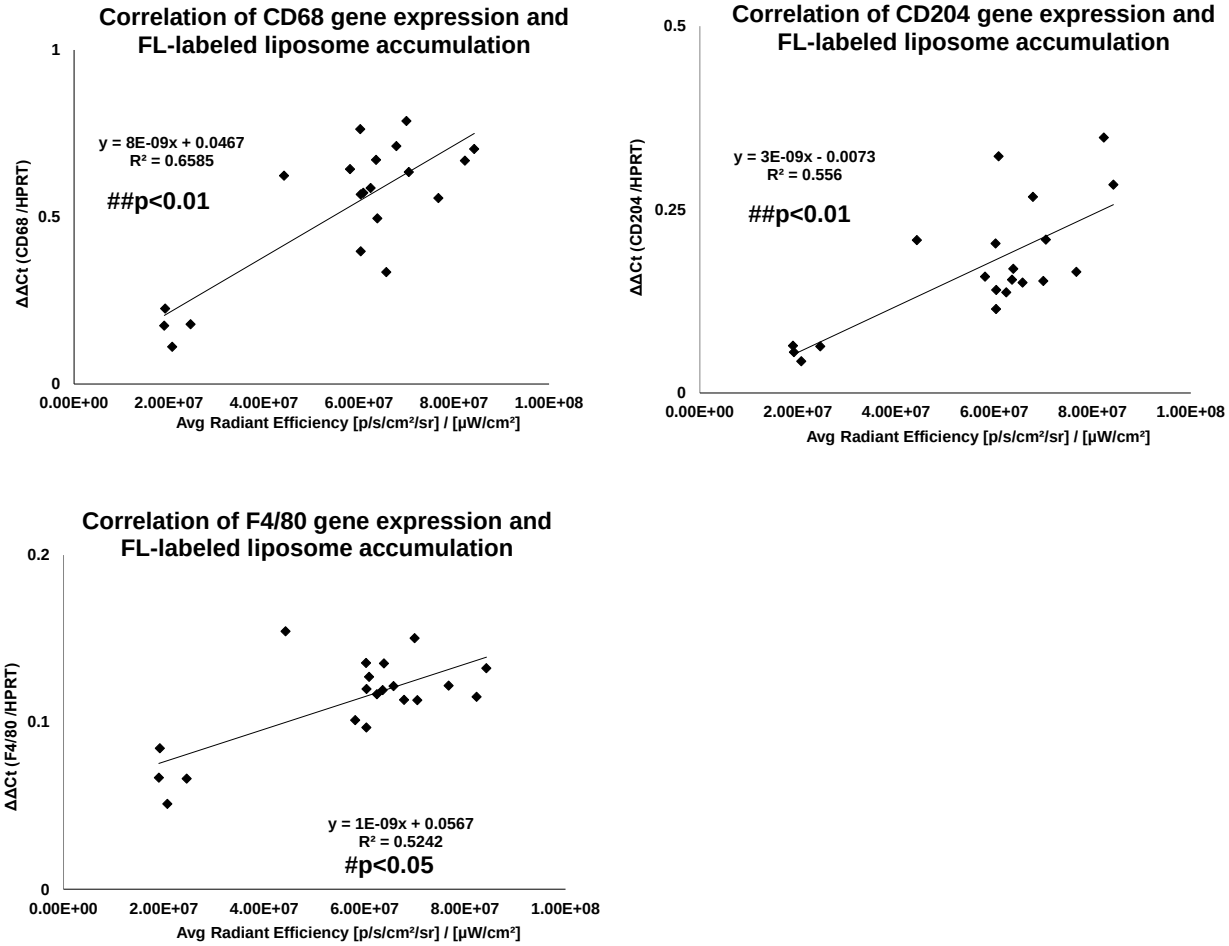


**Figure 3.11 Correlation between macrophage markers (CD68, CD204 and F4/80) and fluorescence intensity in the colon tissues of mice.**

A statistical analysis was performed between the DiR-labeled and liposome-treated score 0–4 mouse groups (n = 4, each). # $p < 0.05$ and ## $p < 0.01$ by Spearman correlation.

### 3.4 Discussion

The author investigated the biodistribution of FL-labeled liposomes after intravenous administration in the IBD mouse model to explore the advantage of nanoparticles. Recent studies using imaging methods indicated that the intravenous administration of ~200 nm-sized nanoparticles results in their accumulation in the colons of mice with colitis. Watanabe et al. demonstrated that ~110 nm is the optima size for targeting the colon and that dextran sulfate sodium (DSS) induced colitis in the mouse model [44]. The three major types of mouse colitis models are presented in Table 3.2. It has been suggested that the DSS-induced colitis mouse model poorly mimics human IBD because DSS induces breakdown of the mucosal barrier without crucial immune cell involvement. In chronic IBD, more complicated pathological conditions occur, such as T helper 17 cells and regulatory T cells [45]. Therefore, it is important for one to select the most appropriate animal model to evaluate the relationship between nanoparticles at the accumulation and injury sites. In this study, the author detected a strong correlation between the accumulation of FL-labeled liposomes and colitis disease state in the T-cell transfer IBD mouse model. In typical experimental IBD animal models, disease severity is often correlated with the activity of myeloperoxidase (MPO) and higher levels of pro-inflammatory cytokines. MPO activity can be used as a surrogate marker of inflammation [46]. MPO plays a role as a major enzymatic catalyst of lipid peroxidation, contributing to the production of ROS in conjunction with the nicotinamide adenine dinucleotide phosphate-oxidase enzyme. Intravenously injected liposomes and micelles are recognized by macrophages and are eventually trapped by the RES in the liver, spleen, and lymph nodes [47]. The author demonstrated that the fluorescent intensity of the FL-labeled liposome was positively correlated with the levels of macrophage marker gene expression.

Recently, macrophages were categorized into two types: inflammatory (M1) and resolving (M2) macrophages. M1 cells are thought to play a role in prototypic inflammatory response, whereas M2 cells are thought to play a role in inflammation resolution and tissue remodeling [48]. Hoppstädter J et al. suggested that nanoparticle (<41 nm) uptake by M2 macrophages was enhanced compared with that by M1 macrophage. Moreover, these findings were not observed in micro-sized particles [49]. In the gastrointestinal epithelial barrier, M2 macrophages play a crucial role in the host gut environment. M2 macrophages downregulate excessive anti-inflammatory reaction in response to bacterial products, such as short-chain fatty acids [50]. The characteristics of these M2 macrophages can be adopted in the treatment strategy against IBD. In other words, the activation of drug-encapsulating nanoparticles by M2 macrophages is an attractive formulation for the improvement of IBD treatment. However, further research is warranted to identify the type of macrophages that uptake nanoparticles and determine the contribution of other types of immune cells (e.g., lymphocytes). In conclusion, the nanoparticle formulation strategy is promising for the treatment of cancer and other conditions, such as IBD.

Apigenin is a flavone compound abundantly found in plants (e.g., *Dracocephalum kotschyi, Matricaria recutita L, and Olea europaea*). Its antioxidant, anti-inflammatory, and anti-cancer activities have been previously stated. The study conducted by Sadraei et al. indicated that apigenin has an inhibitory effect on myeloperoxidase activities in acetic-acid-induced colitis mouse models, providing similar efficacy to that of prednisolone [51]. Additionally, Isoda et al. demonstrated that apigenin, oleuropein, and luteolin in Picholine olive oil inhibit several important inflammatory signaling pathway molecules, such as AKT and TNF, in a rat basophilic leukemia mast

cell line [52]. Notably, this group demonstrated the anticancer effect of ethanolic extracts containing tyrosol, hydroxytyrosol, oleuropein, rutin, quercetin, and glucoside forms of luteolin and apigenin from olive fruitsin human colon cancer cell lines [53]. Moreover, Radulovic et al. suggested that apigenin improves microbiome diversity via an inflammasome independent pathway in dextran sulfate sodium-induced mouse colitis. Collectively, natural products (e.g., polyphenols and flavonoids) prevent the functional impairment of intestinal epithelial cells, concomitant with inflammation of the lamina propria through direct anti-inflammatory effects and indirect therapeutic effects, including improvement of the gut microbiome environment. In Chapter 4, the author presents a feasibility study for the manufacturing of a natural product-encapsulating nanoparticle.

Following the contents of Chapter 1,2, and 3, the author tried manufacturing of nanoparticle encapsulated natural product derived compound as apigenin nanoparticle in the Chapter 4. In addition, the inhibitory effect of this formulation was investigated in mouse macrophage cell line.

# Chapter 4 Formulation approach for natural products in IBD

## 4.1 Introduction

In this Chapter, the author proposed novel formulation optimization strategies for natural products using DDS. Although natural products possess diverse pharmacological activities, occasionally, utilization as a bioactive substance is limited owing to the lack of efficacy, pharmacokinetic problems, and adverse effects. Since apigenin and luteolin exhibit poor solubility and/or low oral bioavailability, significant pharmacokinetic improvement will be expected by the formulation approach.

Owing to the hydrophobicity of apigenin, the liposomal or PLGA (Poly lactic-co-Glycolic Acid) formulation is considered a powerful option for formulation optimization. Similarly, rosmarinic acid is an alcohol-soluble compound, and liposomal formulation is a possible approach. In addition, rosmarinic acid contains a carboxylic acid, which is represented by the general formula R-COOH. The carboxylic acid makes it possible to combine various kinds of hydrophobic groups. In case of water-insoluble compounds, such as oleuropein, a different approach is required. For example, the water in oil water method is an effective manufacturing method for water-insoluble compounds in nanoparticle formulation.

In recent years, nanoparticle formulation approaches for these natural products have been investigated by several studies. These research studies suggested that apigenin and luteolin nanoparticles (liposome and PLGA) for the specific targeting of inflammation sites and cancer are promising. The *in vitro* and *in vivo* stabilities of these nanoparticles are sufficient for these evaluations [54]. Indeed, numerous studies have reported apigenin-, luteolin-, and rosmarinic acid-encapsulating nanoparticles (Table 4.1). These reports targeted a wide range of diseases and formulations. The versatility of nanoparticles was suggested in this study. Moreover, modification of the nanoparticle surface and encapsulation of multiple ingredients is possible depending on the properties

of the materials. Theoretically, various antibodies, peptides, and nucleic acids can be selected as materials for surface modification. Moreover, a couple of natural products can be selected as payload. This attractive approach realizes novel formulation manufacturing, such as both apigenin- and luteolin-encapsulating surface-modified nanoparticles with available therapeutic antibodies (e.g., TNF-α antibody) and/or peptides (e.g., IL-22).

**Table 4.1 Current formulation approaches against natural compounds.**

<table>
<tr><th>Natural products</th><th>Oral</th><th>Intravenously or intraperitoneal</th><th>Inhalation or intranasal</th><th>in vitro</th></tr>
<tr><td rowspan="6">Apigenin</td><td rowspan="6">(C) Nanosuspension[55]</td><td rowspan="3">(C) PLGA[56]</td><td rowspan="6">(IM) Bovine serum albumin nanoparticles [57]</td><td>(C)The apigenin-loaded sodium hyaluronate nano-assemblies [58]</td></tr>
<tr><td>(I) Silver nanoparticles [59]</td></tr>
<tr><td>(IM) Biodegradable polymer carrier [60]</td></tr>
<tr><td rowspan="3">(C) PLGA nanoparticles[55]</td><td>(IM) Degradable poly (apigenin) polymer [61]</td></tr>
<tr><td>(C) PLGA [62]</td></tr>
<tr><td>(C)Apigenin loaded lipid nanocapsules [63]</td></tr>
<tr><td rowspan="3">luteolin</td><td rowspan="3">-</td><td>(C) Luteolin-loaded micelles [64]</td><td rowspan="3">-</td><td rowspan="2">(C,IM) Gold nanoparticles [65]</td></tr>
<tr><td>(C) Water-soluble polymer-encapsulated nano-luteolin [66]</td></tr>
<tr><td>(C) Monomethoxy poly(ethylene glycol)-poly(e-caprolactone) micelles to encapsulate luteolin [67]</td><td>(C,I) mPEG-luteolin-silver nanoparticles [68]</td></tr>
<tr><td rowspan="5">Rosmarinic acid</td><td rowspan="5">-</td><td rowspan="5">-</td><td rowspan="5">(N) Optimized rosmarinic acid-loaded solid lipid nanoparticles using tween 80 [69]</td><td>(N)Rosmarinic acid- and curcumin-loaded polyacrylamide-cardiolipin-poly(lactide-co-glycolide) nanoparticles with conjugated 83-14 monoclonal antibody [70]</td></tr>
<tr><td>(N)Rosmarinic acid-loaded polyacrylamide-chitosan-poly(lactide-co-glycolide) nanoparticles and surface DSPE-PEG(2000) nanoparticles [71]</td></tr>
<tr><td>(IM) Solid nanoparticles produced with two different waxes loaded with rosmarinic acid [72]</td></tr>
<tr><td>(IM) Rosmarinic acid loaded chitosan nanoparticles [73]</td></tr>
<tr><td>(MB) Solid nanoparticles produced with two different waxes loaded with rosmarinic acid [74]</td></tr>
</table>

* The words in parentheses are targeted diseases; **C**:cancer, **I**:infection, **IM**:inflammation, **N**:nurve system and **MB**:microbiome

## 4.2 Materials and methods

### 4.2.1 Nanoparticle manufacturing

Apigenin (>98% purity, TOKYO CHEMICAL INDUSTRY CO., LTD., Ja pan), 1,2-Dimyristoyl-rac-glycerol (GM-020, NOF CORPORATION, Japan), 1,2-Di palmitoyl-sn-glycero-3-phosphocholine (DPPC, NOF CORPORATION, Japan), Cho lesterol(Avanti Polar Lipids, Inc. USA) and 1,2-Dioleoyloxy-3-trimethylammonium propane (DOTAP, NOF CORPORATION, Japan) were used as materials of nano particles. apigenin was dissolved in 90% ethanol (EtOH), 10% water at 172 μg/ ml with lipids at mixing molar ratio shown in Table 4.2. 1.5 ml of apigenin an d lipid mixturewas mixed with 7.5 ml of 10 mM borate buffer pH 9 in a micro fluidic mixer NanoAssemblr (PRECISION NANOSYSTEMS, USA) to form nano particles. Resulting nanoparticle dispersion was dialyzed with dialysis membrane of MWCO 20 k against PBS for 24 hours at 4 ℃. The nanoparticle was stored at 4 ℃ before use. apigenin concentrations of each nanoparticle formulation were determined by colorimetric analysis of measuring optical absorbance at 405 nm after dissolving in 10% borate EtOH solution. Scattered light intensity, diameters and zeta-potential of nanoparticles were measured by static, dynamic and electrop horetic light scattering analysis method with Zetasizer Nano ZS (Malvern Panalyt ical, UK).

**Table 4.2 Components of nanoparticles.**

| | ① Apigenin nanoparticle | ② Empty nanoparticle | ③ DOTAP(-) nanoparticle | ④ Apigenin solution |
|---|---|---|---|---|
| Apigenin | 5 | 0 | 5 | 5 |
| GM-020 | 2 | 2 | 2 | 0 |
| DPPC | 33 | 33 | 33 | 0 |
| Cholesterol | 30 | 30 | 30 | 0 |
| DOTAP | 30 | 30 | 0 | 0 |

Component ratio of each formulation are shown as percentage by moles (Mol%).

### 4.2.2 Gene expression analysis of inflammation related marker in LPS-stimulated RAW264.7 cell line

RAW264.7 cell line (American Type Culture Collection, USA) was seeded at a density of $2 \times 10^5$ cells/1 well/12 well plate in Dulbecco's Modified Eagle's Medium (Invitrogen, US) with 10% fetal bovine serum containing 100 U Penicillin-Streptomycin (Invitrogen, US). All formulations were added with cell seeding at the same time and incubated in an atmosphere of 95% air and 5% $CO_2$ at 37°C for 24 h. Cells were stimulated by LPS (5ng/mL) for 4h and lysed at in the lysis buffer provided in the RNeasy mini kit (Qiagen, Germany). Total RNA was purified using the RNeasy mini kit according to the manufacturer's instructions. Complimentary DNA (cDNA) was synthesized using reverse transcription (RT, SuperScript® VILO™ cDNA synthesis kit**,** Life Technologies, USA) using isolated total RNA as a template. The mRNA expression levels were measured using quantitative real-time RT-polymerase chain reaction using the quantitative PCR MASTER MIX (Nippon Gene, Japan) and ABI 7900HT (Life Technologies, USA) with the target mRNA specific primer and probe sets listed in Table 4.3 Each mRNA expression level was calculated using the $\mathbf{2^{-\Delta Ct}}$ method according to the manufacturer's instruction, and mRNA expression levels of IL-1β, TNF-α, Nlrp3, IL-6 and GAPDH were normalized to mRNA expression levels as an internal control.

### 4.2.3 Statistical analysis

For two groups comparison, Student's t-test or Aspin-welch test was used, P-values < 0.05 were considered statistically significant.

## 4.3. Results

### 4.3.1 Confirmation of solubility in EtOH and nanoparticle formulation

Since apigenin aggregates in aqueous solutions, it is difficult to administer systemically for in vivo study and clinical use. To investigate aggregation behavior of apigenin in polar solvent, apigenin was dissolved in EtOH and then diluted with varied ratio of water, followed by scattered light intensity measurement to detect formation of aggregates. Apigenin could be dissolved in 100% EtOH completely, while precipitated at EtOH concentration lower than 30% (Figure 4.1). Based on this result, four nanoparticle formulations were manufactured by ethanol dilution method (Figure 4.2).

A cationic lipid DOTAP was selected as one of components of nanoparticle to facilitate nanosized co-precipitation of anionic apigenin with the other nanoparticle components. As a result, Z-average diameter of apigenin containing nanoparticle was 37 nm with polydispersity index 0.345, while Z-average diameter of apigenin dispersion without nanoparticle components was as large as 1632 nm and polydispersity index 1, almost out of the range of size distribution measurement by dynamic light scattering method (Table 4.4). Regarding a formulation without DOTAP, neither Z-average diameter nor polydispersity index indicated deposition of apigenin, however, significant amount of deposition was observed in the bottom of test tube by visual inspection (Figure 4.2).

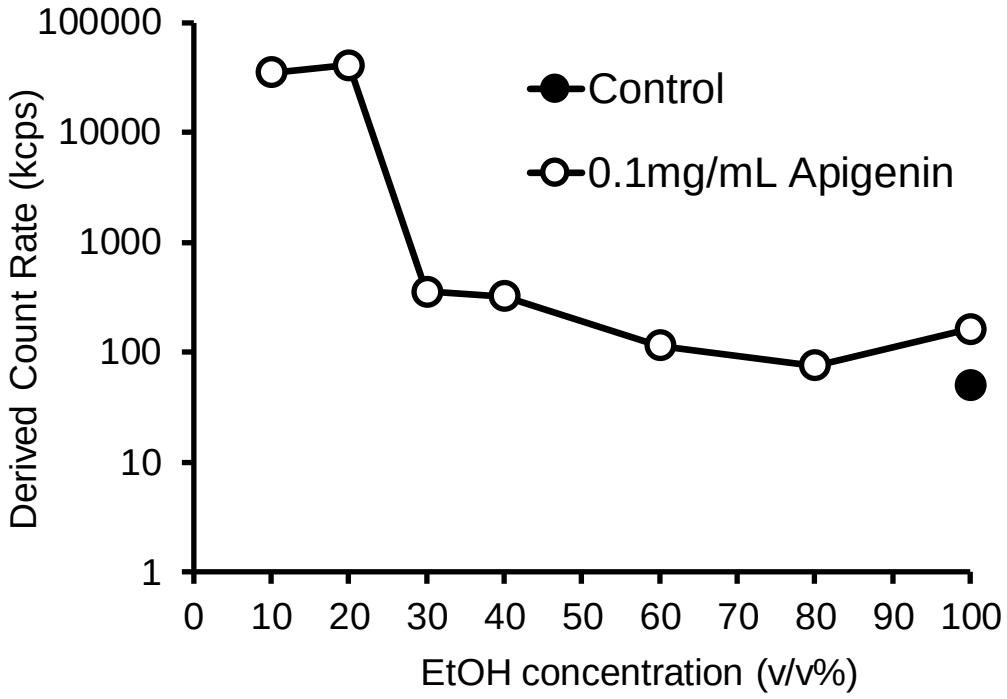


**Figure 4.1 Apigenin solubility in various ethanol concentration.**

Apigenin was dissolved in EtOH and diluted with varied ratio of water.

**Table 4.2 Formulation characteristic parameter.**

| Sample | Z-average diameter (nm) | Polydispersity index |
|---|---|---|
| ① Apigenin nanoparticle | 37 | 0.345 |
| ② Empty nanoparticle | 35 | 0.33 |
| ③ DOTAP(-) nanoparticle | 60 | 0.156 |
| ④ Apigenin solution | 1632 | 1 |

Z-average diameter and polydispersity index of each formulation.

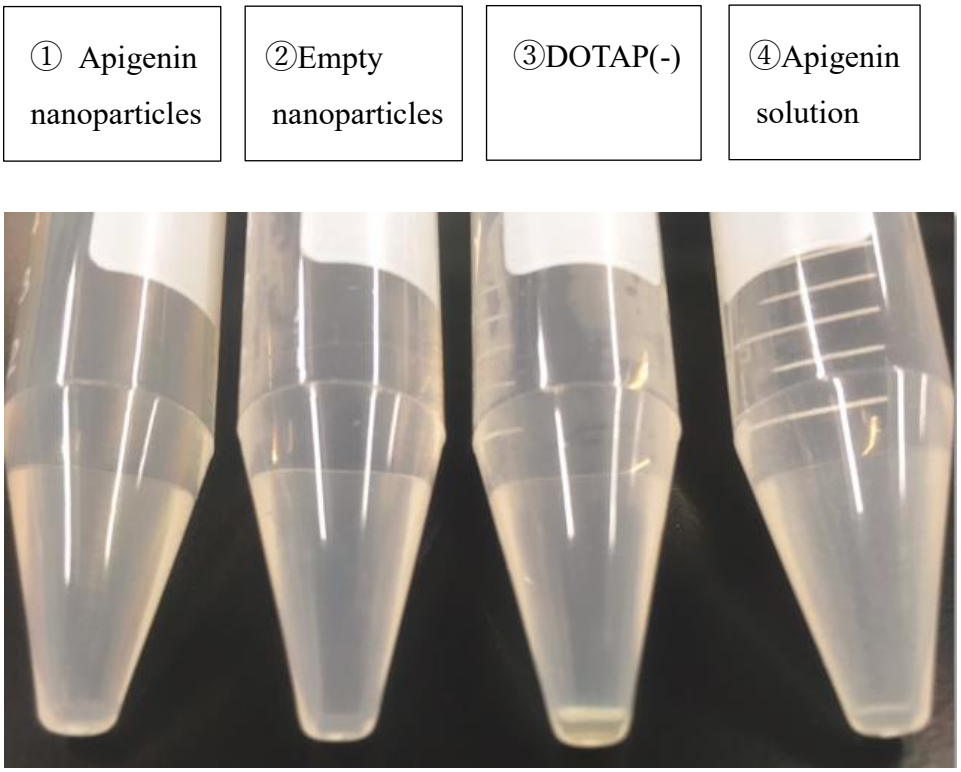


**Figure 4.2 Sample appearance in the 15mL tube at 1 week after manufacturing.**

Amount of deposition was observed in the bottom of test tube by visual inspection in ③ and ④.

### 4.3.2 Enhanced anti-inflammatory effect by apigenin nanoparticles in LPS-stimulated RAW264.7 cell line

Our preliminary studies demonstrated that apigenin could dissolve completely in 100% Dimethyl Sulfoxide (DMSO) solution which is one of the strongest organic solvents. However apigenin made precipitates under low DMSO concentration condition such as buffer solution and basal medium, which means therapeutic effect of apigenin could not be estimated exactly. In this study, apigenin solution made precipitates in the synthesis process as the author expected, on the other hand apigenin nanoparticle endured the use in evaluation. IL-1β and TNF-α are typical inflammatory mediators in IBD, in addition IL-6 drives Th17 differentiation of naïve T cells, it exacerbates inflammation in the gut[43]. Nlrp3 inflammasome is also deeply involved in IBD disease progression, previous study suggested that suppressing Nlrp3 activation prevented gut inflammation[43]. Apigenin nanoparticle had a stronger inhibitory effect on these gene expression levels compared with apigenin solution significantly (Figure 4.3). Unexpectedly, empty nanoparticle in itself inhibited elevation of LPS-induced these gene expression levels strongly, it was suggested that this nanoparticle materials have potent anti-inflammatory effect in this model.

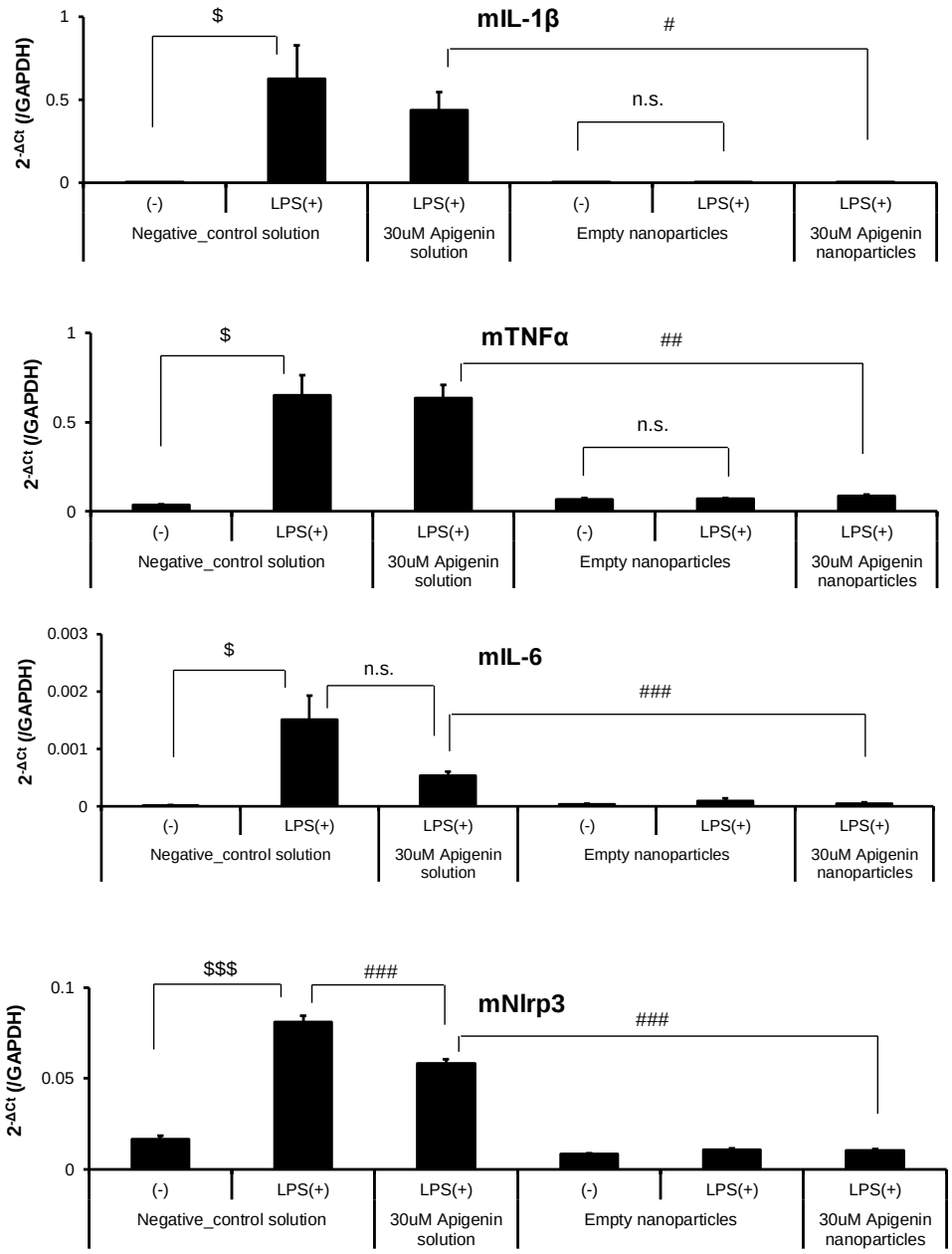


**Figure 4.3 Anti-inhibitory effect of apigenin nanoparticle on LPS stimulated RAW264.7 cell line.**

Data are expressed as mean + SD (n = 3) $ $p < 0.05$ and $$$ $p < 0.001$ by Student's t-test or Aspin-welch t-test. Data are expressed as mean + SD (n = 3) # $p < 0.05$, ##$p < 0.01$ and ###$p < 0.001$ by Student's t-test or Aspin-welch t-test.

## 4.4 Discussion

Previous reports suggest that apigenin could be encapsulated successfully such as liposome, lipid nanocapsule and polymeric nanocapsule [75]. To realize clinical apigenin indication with DDS, formulation approach is necessary, especially strategy for overcoming hydrophobicity against aqueous solution is important. As described, this formulation with DOTAP could avoid precipitation, it kept in culture medium. The most likely mechanism of nanoparticle assembly is reaction between de-protonated anionic apigenin at pH9 and cationic DOTAP, thus apigenin-DOTAP co-precipitates in nanoparticle (Figure 4.4).

It is presumed that cationic lipid such as dimethyldioctadecylammomium bromide (DDAB), DOTAP, 3-tetradecylamino-*N*-tert-butyl-*N*′-tetradecylpropionamidine (DiC14-amidine), dimyristoyltrimethylammonium propane (DMTAP) or dimethylaminoethanecarbamoyl cholesterol (DC-Chol) has anti-inflammatory activity *in vitro* or *in vivo* model[76]. Filion et al. proved that these cationic lipids inhibited swelling of footpad inflammation induced by carrageenan or by sheep red blood cell challenge, moreover they suggested that these mechanism might be involved in blockade of IL-6 and TNF-a in the cytoplasm after macrophage phagocytosis [77]. Concentration of cationic lipid in this article corresponded fairly closely to cationic lipid of this nanoparticle concentrations. Elouahabi A et al. demonstrated that free diC14-amidine liposome injected to mice may be preferentially taken up by macrophages, resulting in a decrease in their ability to respond to stimulation by the CpG motifs contained in diC14-amidine/protamine/pCMV-luc complex and consequently to secrete TNF-α[76]. As was the studies for previous reports, our studies suggested that cationic lipids are potent inhibitors of the LPS-induced inflammatory response through macrophage phagocytosis. The mechanism of anti-inflammatory effect of cationic liposome may be involved in

protein kinase C (PKC) activity. Previous reports suggest that one of the cationic lipid, amphiphiles possesses inhibitory effects against PKC [78]. Hence, it is hypothesized that cationic liposome block the molecule of downstream signaling pathway of PKC, such as NFκB activation, it leads downregulation of TNF-α, IL-1β, IL-6 and NO. Meanwhile, it is seemed that apigenin has several important inflammatory signaling pathway molecules such as AKT and TNF as above[52]. Besides these effects, inhibition of inflammasome mediated pathway is considered as one of the blockade mechanisms of macrophage activation[79]. Here, the author proved that apigenin inhibited Nlrp3 gene expression levels in LPS-stimulated RAW264.7 cell line model. In fact, apigenin its own possesses inhibitory effects against inflammasome through inhibition of the oligomerization of apoptosis-associated speck like protein containing a caspase recruitment domain [37], nanoparticle formulation make it possible to enhance the effect sufficiently because nanoparticles are uptaken by macrophage through phagocytosis (Figure 4.6). In consideration of our results, anti-inflammatory effect of apigenin could not be assessed exactly because cationic lipid nanoparticles have powerful anti-inflammatory effects, thus it was difficult to judge whether additive or synergistic effect could be achieved or not. Nevertheless, this formulation made it possible to be sufficient totreat *in vitro* and *in vivo* study. Additional work is needed to show proof of concept.

Inflammasome and these inflammatory cytokine activation are associated with increased risk for the development of several disorders besides IBD, such as erythematosus, rheumatoid arthritis and diabetes [80], these findings suggests that apigenin nanoparticle is attractive therapeutic option for these refractory diseases.

In conclusion, apigenin nanoparticle could be manufactured successfully, the nanoparticles showed strong efficacy. According to our results, cationic lipid on its own

has powerful anti- inflammatory effects, these findings suggest that nanoparticle encapsulated natural product can be a promising formulation for inflamed tissues.

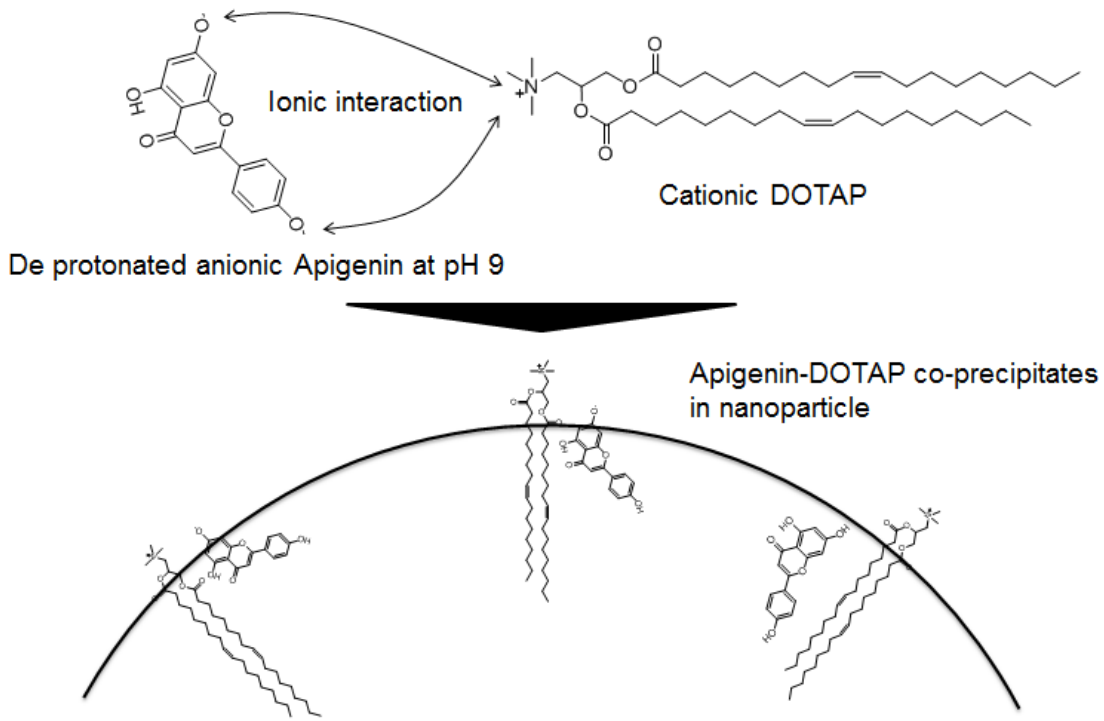


**Figure 4.4 Diagram of nanoparticle assembly with apigenin and DOTAP.**

Reaction between de-protonated anionic apigenin at pH9 and cationic DOTAP.

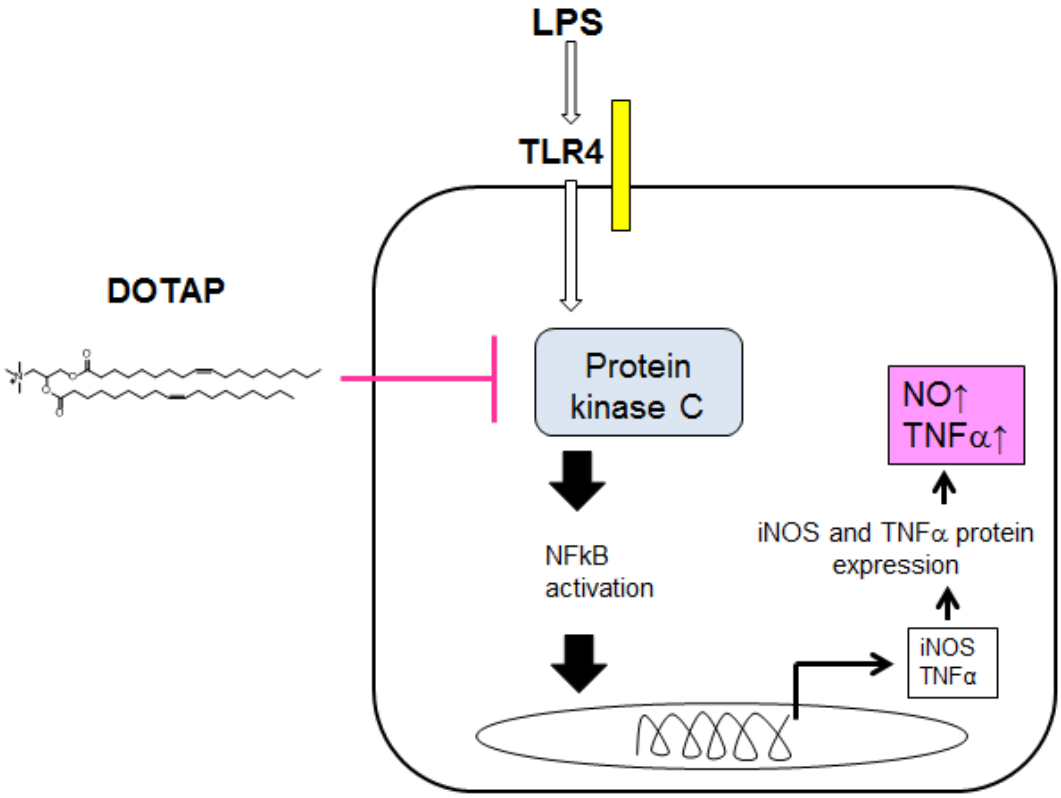


**Figure 4.5 Hypothesis of Mechanism of Inhibitory Effect of DOTAP on NO and TNFα Production.**

Cationic lipid block the molecule of downstream signaling pathway of PKC, such as NFκB activation, it leads downregulation of TNF-α and NO.

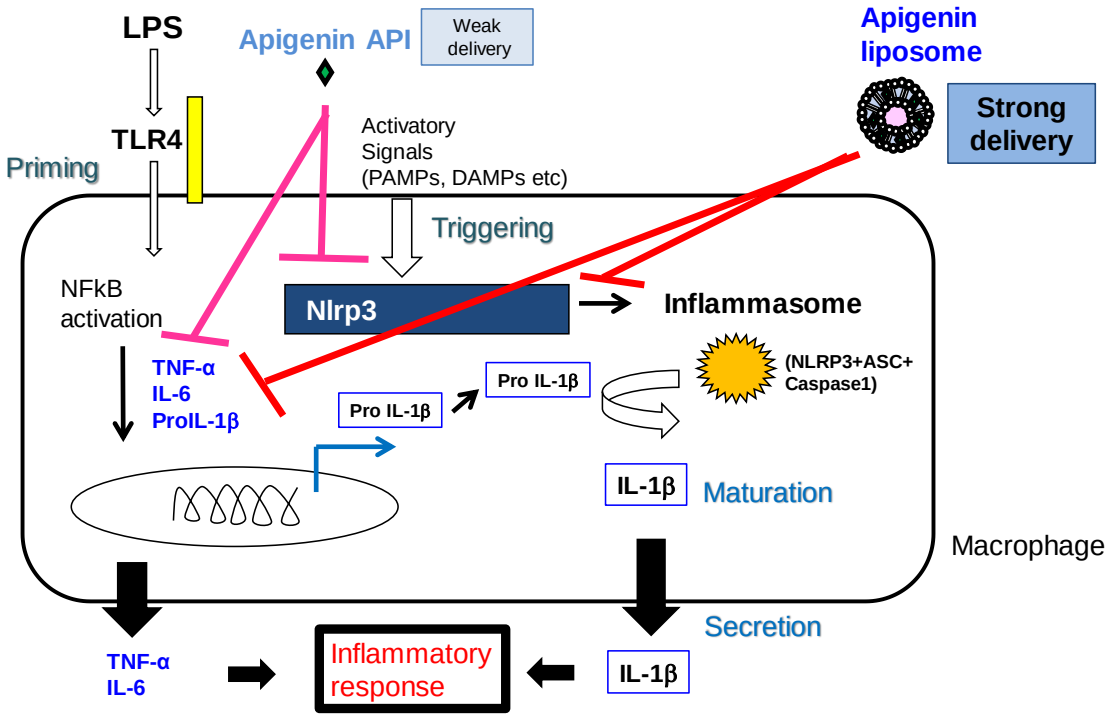


**Figure 4.6 Hypothesis of mechanism of strong effect of Apigenin liposome.**

Nanoparticles uptake by macrophage through phagocytosis enhance the anti-inflammatory effect sufficiently due to both blockade of downstream signaling pathway of PKC by cationic liposome and inhibition of important inflammatory signaling such as AKT and TNF.

# Chapter 5 General conclusions

Natural products such as polyphenol or flavonoids derivatives have an inhibitory effect of abnormal immune cells activation in colitis tissue, it leads mucosal epithelial barrier protection. Additionally, these ingredients have a potential to improve intestinal microbiome diversity, consequently bacterial metabolites play an important role of keeping environmental homeostasis. These findings suggest that natural products have a potential to ameliorate colon inflammation.

In Chapter 2, the author selected appropriate liposome to deliver for inflammatory region using MCT model, and proved that liposome accumulation was correlated with severity of vascular permeability, in other words, this liposome accumulated in injured tissue through EPR effect. In Chapter 3, the author evaluated potential to accumulation of liposome for colitis model. The results showed that specific accumulation at the colon was observed in T cell transfer IBD mouse model, liposome delivery in accordance with pathological severity was demonstrated. Moreover, liposome accumulation was correlated with macrophage related gene marker expression levels, it is suggested that this liposome can be a promising formulation for delivery to the injured IBD tissue specifically. In Chapter 4, the formulation approach of natural products for IBD was proposed using DDS technology, moreover the possibility for modification of nanoparticle formulation was suggested.

In conclusion, important findings for the development of the future treatment for IBD based on environmental changes were obtained, moreover natural product encapsulated therapeutic nanoparticles for social implementation was manufactured successfully. This formulation strategy might be able to give new treatment options for inflammatory disease patients.

**Acknowledgements**

First of all, I would like to express my deepest appreciation to my supervisor, Prof. Hiroko Isoda. I would like to express my gratitude to Prof. Zhang Zhenya, Prof. Myra Orlina Villareal and Prof. Yusaku Miyamae. Advice and comments given by Isoda lab members has been a great help in my work. I appreciate Research Manager Atsushi Nakanishi and Associated Director Hirokazu Matsumoto (supervisors of the author) to approve to study in University of Tsukuba. Special thanks to Yo Muraki, Satoru Matsumoto, and Sabti Mouad.

**References**


1. Natalie A. Molodecky, B., and Gilaad G. Kaplan, MD, MPH, FRCPC, *Environmental Risk Factors for Inflammatory Bowel Disease.* Gastroenterology & Hepatology, 2010. **6**(5).

2. Rogler, G., L. Biedermann, and M. Scharl, *New insights into the pathophysiology of inflammatory bowel disease: microbiota, epigenetics and common signalling pathways.* Swiss Med Wkly, 2018. **148**: p. w14599.

3. Scaioli, E., E. Liverani, and A. Belluzzi, *The Imbalance between n-6/n-3 Polyunsaturated Fatty Acids and Inflammatory Bowel Disease: A Comprehensive Review and Future Therapeutic Perspectives.* Int J Mol Sci, 2017. **18**(12).

4. Haskey, N. and D.L. Gibson, *An Examination of Diet for the Maintenance of Remission in Inflammatory Bowel Disease.* Nutrients, 2017. **9**(3).

5. Bastida, G. and B. Beltran, *Ulcerative colitis in smokers, non-smokers and ex-smokers.* World J Gastroenterol, 2011. **17**(22): p. 2740-7.

6. Wang, Q., et al., *Aryl hydrocarbon receptor inhibits inflammation in DSSinduced colitis via the MK2/pMK2/TTP pathway.* Int J Mol Med, 2018. **41**(2): p. 868-876.

7. Kumar, M., et al., *Human gut microbiota and healthy aging: Recent developments and future prospective.* Nutr Healthy Aging, 2016. **4**(1): p. 3-16.

8. Sartor, R.B. and G.D. Wu, *Roles for Intestinal Bacteria, Viruses, and Fungi in Pathogenesis of Inflammatory Bowel Diseases and Therapeutic Approaches.* Gastroenterology, 2017. **152**(2): p. 327-339 e4.

9. Omar, S.H., *Oleuropein in olive and its pharmacological effects.* Sci Pharm, 2010. **78**(2): p. 133-54.

10. Jin, B.R., et al., *Rosmarinic acid suppresses colonic inflammation in dextran sulphate sodium (DSS)-induced mice via dual inhibition of NF-kappaB and STAT3 activation.* Sci Rep, 2017. **7**: p. 46252.

11. Salaritabar, A., et al., *Therapeutic potential of flavonoids in inflammatory bowel disease: A comprehensive review.* World J Gastroenterol, 2017. **23**(28): p. 5097-5114.

12. Wan, L., et al., *Quantitative determination of apigenin and its metabolism in rat plasma after intravenous bolus administration by HPLC coupled with tandem mass spectrometry.* J Chromatogr B Analyt Technol Biomed Life Sci, 2007. **855**(2): p. 286-9.

13. Rose-Jones, L.J. and V.V. McLaughlin, *Pulmonary hypertension: types and treatments.* Curr Cardiol Rev, 2015. **11**(1): p. 73-9.

14. Gomez-Arroyo, J.G., et al., *The monocrotaline model of pulmonary hypertension in perspective.* Am J Physiol Lung Cell Mol Physiol, 2012. **302**(4): p. L363-9.

15. Nogueira-Ferreira, R., et al., *Exploring the monocrotaline animal model for the study of pulmonary arterial hypertension: A network approach.* Pulm Pharmacol Ther, 2015. **35**: p. 8-16.

16. Zheng, X., et al., *Developments in drug delivery of bioactive alkaloids derived from traditional Chinese medicine.* Drug Deliv, 2018. **25**(1): p. 398-416.

17. Maeda, Y.M.a.H., *A new concept for macromolecular therapeutics in cancer chemotherapy: mechanism of tumoritropic accumulation of proteins and the antitumor agent smancs.* CANCER RESEARCH, 1986. **46**(12 Pt 1): p. 6387-6392.

18. He, C., et al., *Effects of particle size and surface charge on cellular uptake and biodistribution of polymeric nanoparticles.* Biomaterials, 2010. **31**(13): p. 3657-66.

19. Suk, J.S., et al., *PEGylation as a strategy for improving nanoparticle-based drug and gene delivery.* Adv Drug Deliv Rev, 2016. **99**(Pt A): p. 28-51.

20. Muraki, Y., et al., *Fluorescent Imaging Analysis for Distribution of Fluorescent Dye Labeled- or Encapsulated-Liposome in Monocrotaline-Induced Pulmonary Hypertension Model Rat.* Chem Pharm Bull (Tokyo), 2018. **66**(3): p. 270-276.

21. Asghar, M.N., et al., *In vivo imaging of reactive oxygen and nitrogen species in murine colitis.* Inflamm Bowel Dis, 2014. **20**(8): p. 1435-47.

22. Liu, D., A. Mori, and L. Huang, *Role of liposome size and RES blockade in controlling biodistribution and tumor uptake of GM1-containing liposomes.* Biochim Biophys Acta, 1992. **1104**(1): p. 95-101.

23. Kraft, J.C., et al., *Emerging research and clinical development trends of liposome and lipid nanoparticle drug delivery systems.* J Pharm Sci, 2014. **103**(1): p. 29-52.

24. Rosse, W.F., *The spleen as a filter.* N Engl J Med, 1987. **317**(11): p. 704-6.

25. Liu, D., A. Mori, and L. Huang, *Large liposomes containing ganglioside GM1 accumulate effectively in spleen.* Biochim Biophys Acta, 1991. **1066**(2): p. 159-65.

26. Takemoto, K., et al., *Comparative study on the efficacy of AmBisome and Fungizone in a mouse model of pulmonary aspergillosis.* J Antimicrob Chemother, 2006. **57**(4): p. 724-31.

27. Oku, N., *Innovations in Liposomal DDS Technology and Its Application for the Treatment of Various Diseases.* Biol Pharm Bull, 2017. **40**(2): p. 119-127.

28. Martinez-Montiel, M.P., et al., *Pharmacologic therapy for inflammatory bowel disease refractory to steroids.* Clin Exp Gastroenterol, 2015. **8**: p. 257-69.

29. MUNKHOLM, P., *Review article: the incidence and prevalence of colorectal cancer in inflammatory bowel disease.* Aliment Pharmacol Ther 2003; 18 (Suppl. 2): 1–5., 2003. **18**(Suppl.2): p. 1-5.

30. Cristina CI JEVSCHI PRELIPCEAN, C.M., Petruţ GOGALNI CEANU, Bogdan MIHAI, *What is the impact of age on adult patients with inflammatory bowel disease?* Clujul Medical, 2013. **86**(1).

31. Ng, S.C., et al., *Worldwide incidence and prevalence of inflammatory bowel disease in the 21st century: a systematic review of population-based studies.* The Lancet, 2017. **390**(10114): p. 2769-2778.

32. Zhao, Q. and C.O. Elson, *Adaptive immune education by gut microbiota antigens.* Immunology, 2018. **154**(1): p. 28-37.

33. Donaldson, G.P., S.M. Lee, and S.K. Mazmanian, *Gut biogeography of the bacterial microbiota.* Nat Rev Microbiol, 2016. **14**(1): p. 20-32.

34. Walker, W.A. and R.S. Iyengar, *Breast milk, microbiota, and intestinal immune homeostasis.* Pediatr Res, 2015. **77**(1-2): p. 220-8.

35. Rowland, I., et al., *Gut microbiota functions: metabolism of nutrients and other food components.* Eur J Nutr, 2018. **57**(1): p. 1-24.

36. Levy, M., E. Blacher, and E. Elinav, *Microbiome, metabolites and host immunity.* Curr Opin Microbiol, 2017. **35**: p. 8-15.

37. Ratsimandresey, R.A., A. Dorfleutner, and C. Stehlik, *An Update on PYRIN Domain-Containing Pattern Recognition Receptors: From Immunity to Pathology.* Front Immunol, 2013. **4**: p. 440.

38. CHRISTOPHER J. HAWKEY, L.M.D., LORRAINE V. ROUNTREE, PAUL J. LINNEN, JAMES F. LANCASTER, and THE EUROPEAN ZILEUTON STUDY GROUP FOR ULCERATIVE COLITIS, *A Trial of Zileuton Versus Mesalazine or Placebo in the Maintenance of Remission of Ulcerative Colitis.* GASTROENTEROLOGY, 1997(112): p. 718 –724.

39. Wang, J.W., et al., *Fecal microbiota transplantation: Review and update.* J Formos Med Assoc, 2019. **118 Suppl 1**: p. S23-s31.

40. Yamasaki, M., et al., *Fluorescence-labeled liposome accumulation in injured colon of a mouse model of T-cell transfer-mediated inflammatory bowel disease.* Biochem Biophys Res Commun, 2017. **494**(1-2): p. 188-193.

41. Vasina, V., *Non-peptidyl low molecular weight radical scavenger IAC attenuates DSS-induced colitis in rats.* World Journal of Gastroenterology, 2010. **16**(29).

42. Valatas, V., M. Vakas, and G. Kolios, *The value of experimental models of colitis in predicting efficacy of biological therapies for inflammatory bowel diseases.* Am J Physiol Gastrointest Liver Physiol, 2013. **305**(11): p. G763-85.

43. Strauch, U.G., et al., *Influence of intestinal bacteria on induction of regulatory T cells: lessons from a transfer model of colitis.* Gut, 2005. **54**(11): p. 1546-52.

44. Watanabe, A., et al., *Effect of particle size on their accumulation in an inflammatory lesion in a dextran sulfate sodium (DSS)-induced colitis model.* Int J Pharm, 2016. **509**(1-2): p. 118-22.

45. Kiesler, P., I.J. Fuss, and W. Strober, *Experimental Models of Inflammatory Bowel Diseases.* Cell Mol Gastroenterol Hepatol, 2015. **1**(2): p. 154-170.

46. Kim, J.J., et al., *Investigating intestinal inflammation in DSS-induced model of IBD.* J Vis Exp, 2012(60).

47. Sun, X., et al., *Improved Tumor Uptake by Optimizing Liposome Based RES Blockade Strategy.* Theranostics, 2017. **7**(2): p. 319-328.

48. Kelly, C., C. Jefferies, and S.A. Cryan, *Targeted liposomal drug delivery to monocytes and macrophages.* J Drug Deliv, 2011. **2011**: p. 727241.

49. Hoppstadter, J., et al., *M2 polarization enhances silica nanoparticle uptake by macrophages.* Front Pharmacol, 2015. **6**: p. 55.

50. Isidro, R.A. and C.B. Appleyard, *Colonic macrophage polarization in homeostasis, inflammation, and cancer.* Am J Physiol Gastrointest Liver Physiol, 2016. **311**(1): p. G59-73.

51. Hassan Sadraei, G.A., Mohammad Khanabadi, and Mohsen Minaiyan, *Anti-inflammatory effect of apigenin and hydroalcoholic extract of Dracocephalum kotschyi on acetic acid-induced colitis in rats.* 2017. **12**(4): p. 322-329.

52. Isoda, H., et al., *Antiallergic effect of Picholine olive oil-in-water emulsions through beta-hexosaminidase release inhibition and characterization of their physicochemical properties.* J Agric Food Chem, 2012. **60**(32): p. 7851-8.

53. Maalej, A., et al., *Assessment of Olea europaea L. fruit extracts: Phytochemical characterization and anticancer pathway investigation.* Biomed Pharmacother, 2017. **90**: p. 179-186.

54. Wen-ming Feng, H.-h.G., Tao Xue, Xiang Wang, Cheng-wu Tang, Bao Ying, Hui Gong, Ge Cui, *Anti-inflammation and anti-fibrosis with PEGylated, apigenin loaded PLGA nanoparticles in chronic pancreatitis disease.* RSC Advances, 2015. **5**: p. 83628-83635.

55. Wu, W., et al., *Preparation, characterization and antitumor activity evaluation of apigenin nanoparticles by the liquid antisolvent precipitation technique.* Drug Deliv, 2017. **24**(1): p. 1713-1720.

56. Bhattacharya, S., et al., *Apigenin loaded nanoparticle delayed development of hepatocellular carcinoma in rats.* Nanomedicine, 2018. **14**(6): p. 1905-1917.

57. Papay, Z.E., et al., *Study on the Pulmonary Delivery System of Apigenin-Loaded Albumin Nanocarriers with Antioxidant Activity.* J Aerosol Med Pulm Drug Deliv, 2017. **30**(4): p. 274-288.

58. Zhao, T., et al., *Novel apigenin-loaded sodium hyaluronate nano-assemblies for targeting tumor cells.* Carbohydr Polym, 2017. **177**: p. 415-423.

59. Gurunathan, S., Y.J. Choi, and J.H. Kim, *Antibacterial Efficacy of Silver Nanoparticles on Endometritis Caused by Prevotella melaninogenica and Arcanobacterum pyogenes in Dairy Cattle.* Int J Mol Sci, 2018. **19**(4).

60. Zhang, J., et al., *The potential application of strategic released apigenin from polymeric carrier in pulmonary fibrosis.* Exp Lung Res, 2017. **43**(9-10): p. 359-369.

61. Cochran, D.B., et al., *Degradable poly(apigenin) polymer inhibits tumor cell adhesion to vascular endothelial cells.* J Biomed Mater Res B Appl Biomater, 2016. **104**(7): p. 1438-47.

62. Das, S., et al., *Strategic formulation of apigenin-loaded PLGA nanoparticles for intracellular trafficking, DNA targeting and improved therapeutic effects in skin melanoma in vitro.* Toxicol Lett, 2013. **223**(2): p. 124-38.

63. Ding, B., et al., *Preparation and in vitro evaluation of apigenin loaded lipid nanocapsules.* J Nanosci Nanotechnol, 2013. **13**(10): p. 6546-52.

64. Zheng, S., et al., *Application of luteolin nanomicelles anti-glioma effect with improvement in vitro and in vivo.* Oncotarget, 2017. **8**(37): p. 61146-61162.

65. Gurunathan, S. and J.H. Kim, *Biocompatible Gold Nanoparticles Ameliorate Retinoic Acid-Induced Cell Death and Induce Differentiation in F9 Teratocarcinoma Stem Cells.* Nanomaterials (Basel), 2018. **8**(6).

66. Majumdar, D., et al., *Luteolin nanoparticle in chemoprevention: in vitro and in vivo anticancer activity.* Cancer Prev Res (Phila), 2014. **7**(1): p. 65-73.

67. Qiu, J.F., et al., *Preparation and characterization of monomethoxy poly(ethylene glycol)-poly(epsilon-caprolactone) micelles for the solubilization and in vivo delivery of luteolin.* Int J Nanomedicine, 2013. **8**: p. 3061-9.

68. Qing, W., et al., *Facile synthesis of mPEG-luteolin-capped silver nanoparticles with antimicrobial activity and cytotoxicity to neuroblastoma SK-N-SH cells.* Colloids Surf B Biointerfaces, 2017. **160**: p. 390-394.

69. Bhatt, R., et al., *Development, characterization and nasal delivery of rosmarinic acid-loaded solid lipid nanoparticles for the effective management of Huntington's disease.* Drug Deliv, 2015. **22**(7): p. 931-9.

70. Kuo, Y.C. and H.C. Tsai, *Rosmarinic acid- and curcumin-loaded polyacrylamide-cardiolipin-poly(lactide-co-glycolide) nanoparticles with conjugated 83-14 monoclonal antibody to protect beta-amyloid-insulted neurons.* Mater Sci Eng C Mater Biol Appl, 2018. **91**: p. 445-457.

71. Kuo, Y.C. and R. Rajesh, *Targeted delivery of rosmarinic acid across the blood-brain barrier for neuronal rescue using polyacrylamide-chitosan-poly(lactide-co-glycolide) nanoparticles with surface cross-reacting material 197 and apolipoprotein E.* Int J Pharm, 2017. **528**(1-2): p. 228-241.

72. Madureira, A.R., et al., *Insights into the protective role of solid lipid nanoparticles on rosmarinic acid bioactivity during exposure to simulated gastrointestinal conditions.* Colloids Surf B Biointerfaces, 2016. **139**: p. 277-84.

73. da Silva, S.B., et al., *Chitosan-based nanoparticles for rosmarinic acid ocular delivery--In vitro tests.* Int J Biol Macromol, 2016. **84**: p. 112-20.

74. Madureira, A.R., et al., *Fermentation of bioactive solid lipid nanoparticles by human gut microflora.* Food Funct, 2016. **7**(1): p. 516-29.

75. Karim, R., et al., *Development and evaluation of injectable nanosized drug delivery systems for apigenin.* Int J Pharm, 2017. **532**(2): p. 757-768.

76. Elouahabi, A., et al., *Free cationic liposomes inhibit the inflammatory response to cationic lipid-DNA complex injected intravenously and enhance its transfection efficiency.* Mol Ther, 2003. **7**(1): p. 81-8.

77. Filion, M.C. and N.C. Phillips, *Anti-inflammatory activity of cationic lipids.* Br J Pharmacol, 1997. **122**(3): p. 551-7.

78. Bottega, R. and R.M. Epand, *Inhibition of protein kinase C by cationic amphiphiles.* Biochemistry, 1992. **31**(37): p. 9025-30.

79. Zhang, X., et al., *Flavonoid apigenin inhibits lipopolysaccharide-induced inflammatory response through multiple mechanisms in macrophages.* PLoS One, 2014. **9**(9): p. e107072.

80. Yi, Y.S., *Role of inflammasomes in inflammatory autoimmune rheumatic diseases.* Korean J Physiol Pharmacol, 2018. **22**(1): p. 1-15.